

D.M. Worrall

The X-ray Jets of Active Galaxies

In press — submitted Aug. 31st 2008, revised Nov. 26th 2008

Abstract Jet physics is again flourishing as a result of *Chandra*'s ability to resolve high-energy emission from the radio-emitting structures of active galaxies and separate it from the X-ray-emitting thermal environments of the jets. These enhanced capabilities have coincided with an increasing interest in the link between the growth of super-massive black holes and galaxies, and an appreciation of the likely importance of jets in feedback processes. I review the progress that has been made using *Chandra* and *XMM-Newton* observations of jets and the medium in which they propagate, addressing several important questions, including: Are the radio structures in a state of minimum energy? Do powerful large-scale jets have fast spinal speeds? What keeps jets collimated? Where and how does particle acceleration occur? What is jet plasma made of? What does X-ray emission tell us about the dynamics and energetics of radio plasma/gas interactions? Is a jet's fate determined by the central engine?

Contents

1	The stage is set	2
1.1	Historical perspective	2
1.2	Radiation processes	3
1.3	Generic classes of jets	3
1.4	Lifetimes and duty cycles	5
2	Are the radio structures in a state of minimum energy?	6
2.1	Calculation of the minimum-energy field	6
2.2	Using X-rays to test minimum energy	7
3	Do powerful large-scale jets have fast spinal speeds?	11
3.1	The impetus from PKS 0637-752	11
3.2	The dependence of beamed iC-CMB on beaming factors and redshift	12
3.3	How is the beamed iC-CMB model faring under scrutiny?	13
3.4	Synchrotron emission as an alternative	18

Dept of Physics, University of Bristol, Tyndall Ave, Bristol BS8 1TL, UK
E-mail: d.worrall@bristol.ac.uk

4	What keeps jets collimated?	20
5	Where and how does particle acceleration occur?	22
5.1	The link with synchrotron X-ray emission	22
5.2	Particle acceleration in knotty structures	23
5.3	Incorporating polarization data	24
6	What is jet plasma made of?	25
7	What does X-ray emission tell us about the dynamics and energetics of radio plasma/gas interactions?	28
7.1	Expectations for FRIIs	28
7.2	Dynamics of FRIs in clusters	29
7.3	Centaurus A	30
7.4	The effect of galaxy mergers	31
8	Is a jet's fate determined by the central engine?	32
8.1	An evolutionary cycle?	32
8.2	The rôle played by accretion processes	33
8.3	The rôle of the environment	35
8.4	Information from beamed sources	35
9	Summary and concluding remarks	36

1 The stage is set

1.1 Historical perspective

In the 1970s and 1980s the powerful capabilities of radio interferometry gave birth to the study of extragalactic radio jets. It became clear that radio jets are plasma outflows originating in the centres of active galaxies, seen through their synchrotron emission. After much debate, properties such as the relative one-sidedness of the jets, and the measurement of apparent superluminal expansion, by Very Long Baseline Interferometry (VLBI), were accepted as due to the outflows having relativistic bulk speeds. Early attempts at unifying source populations based on special relativity and apparent source properties [e.g., 175] have developed over the years into comprehensive unified schemes [e.g., 8] whereby quasars are explained as radio galaxies whose jets are at small angles to the line of sight and so are boosted by relativistic effects.

By the mid 1990s, the study of radio jets had reached something of a hiatus, and major groups around the world turned their attention to other pursuits such as gravitational lensing and the study of the Cosmic Microwave Background (CMB) radiation. A turning point was the sensitivity and high-fidelity mirrors of the *Chandra* X-ray Observatory [209], which resulted in the detection of resolved X-ray emission from many tens of well-known extragalactic radio sources (see [103] for a source compilation as of 2006: the number continues to increase). When combined with X-ray measurements of the ambient gas made with *Chandra* and *XMM-Newton*, and multiwavelength data, many important questions related to the physics of jets can be addressed. Progress towards answering those questions is the substance of this review.

The enhanced capabilities for the X-ray study of jets have coincided with strong interest from the wider astronomical community in the growth of super-massive black holes (SMBHs), following the links that have been made between SMBH and galaxy growth [e.g., 165; 79]. SMBHs (and indeed compact objects

of stellar mass) commonly produce jets, as an outcome of accretion processes responsible also for black-hole growth. It is also clear that extragalactic jets are capable of transferring large amounts of energy to baryonic matter in the host galaxies and surrounding clusters at large distances from the SMBH. The way in which heating during the jet mode of AGN activity might overcome the problem of fast radiative cooling in the centre of clusters is now intensely studied in nearby objects (see §7), and heating from ‘radio mode’ activity is included in simulations of hierarchical structure formation [e.g., 57]. We need therefore to understand what regulates the production of jets and how much energy they carry. X-ray measurements of nuclear emission probe the fueling and accretion processes, and those of resolved jet emission and the surrounding gaseous medium probe jet composition, speed, dynamical processes, energy deposition, and feedback.

1.2 Radiation processes

The two main jet radiation processes are synchrotron radiation and inverse-Compton scattering. Their relative importance depends on observing frequency, location within the jet, and the speed of the jet. The thermally X-ray-emitting medium into which the jets propagate plays a major rôle in the properties of the flow and the appearance of the jets. The physics of the relevant radiation processes are well described in published work [e.g., 86; 26; 153; 189; 168; 174; 137], and most key equations for the topics in this review, in a form that is independent of the system of units, can be found in [220].

It is particularly in the X-ray band that synchrotron radiation and inverse-Compton emission are both important. X-ray synchrotron emission depends on the number of high-energy electrons and the strength and filling factor of the magnetic field in the rest frame of the jet. Inverse Compton X-ray emission depends on the number of low-energy electrons, the strength of an appropriate population of seed photons (such as the CMB, low-energy jet synchrotron radiation, or emission from the central engine), and the geometry of scattering in the rest frame of the jet. In an ideal world, observations would be sufficient to determine the emission process, and this in turn would lead to measurements of physical parameters. In reality, X-ray imaging spectroscopy, even accompanied by good measurements of the multiwavelength spectral energy distribution (SED), often leaves ambiguities in the dominant emission process. Knowledge is furthered through intensive study of individual sources or source populations.

1.3 Generic classes of jets

In discussing jets, it is useful to refer to the Fanaroff and Riley [74] classification that divides radio sources broadly into two morphological types, FRI and FR II. A relatively sharp division between FRIs and FR IIs has been seen when sources are mapped onto a plane of radio luminosity and galaxy optical luminosity [136] – the so called Ledlow-Owen relation. FR IIs are of higher radio luminosity, with the separation between the classes moving to larger radio luminosity in galaxies that are optically more massive and luminous. The distinct morphologies [e.g., 150] are believed to be a reflection of different flow dynamics [e.g., 134].

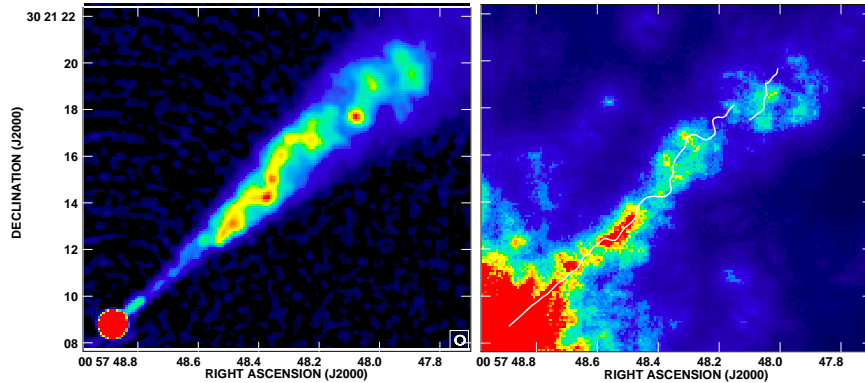


Fig. 1 Roughly 6.6 kpc (projected) of the inner jet of the $z = 0.0165$ FRI radio galaxy NGC 315. Left: 5 GHz *VLA* radio map showing a knotty filamentary structure in diffuse emission. Right: Smoothed *Chandra* X-ray image of ~ 52.3 ks livetime also showing knotty structure embedded in diffuse emission. The ridge-line defined by the radio structure is shown in white, and indicates a level of correspondence between the radio and X-ray knots. Figure adapted from [221].

FRI sources (of lower isotropic radio power, with BL Lac objects as the beamed counterpart in unified schemes) have broadening jets feeding diffuse lobes or plumes that can show significant gradual bending, usually thought to be due to ram-pressure as the source moves relative to the external medium. The jet emission is of high contrast against diffuse radio structures, implying that the jet plasma is an efficient radiator. kpc-scale jets are usually brightest at a flaring point some distance from the active galactic nucleus, and then fade gradually in brightness at larger distances from the core, although this pattern is often interrupted by bright knots seen when the jet is viewed in the radio or the X-ray. Such an example is shown in Figure 1¹. The jets are believed to slow from highly-relativistic to sub-relativistic flow on kpc-scales from entrainment of the external interstellar medium (ISM), perhaps enhanced by stellar mass loss within the jet. The strong velocity shear between the jet flow and the almost stationary external medium must generate instabilities at the interface [20], and drive the flow into a turbulent state. The physics of the resulting flow is far from clear, although it can be investigated with simplifying assumptions [e.g., 14; 15, and see §4].

FRII sources (of higher isotropic radio power, with quasars as the beamed counterpart in unified schemes) have narrower jets that are sometimes faint with respect to surrounding lobe plasma and that terminate at bright hotspots (Fig. 2). The jets are often knotty when observed with high resolution, and the jets can bend abruptly without losing significant collimation (see §3.1 and §5.3 for examples). The bending is often large in quasar jets, supporting the conjecture that quasars are viewed at small angle to the line of sight and that bends are amplified through projection. In contrast to FRI jets which are in contact with the external medium, the standard model for FRII jets is that they are light, embedded in lobe plasma, and remain supersonic with respect to the external gas out to the hotspots. The energy and momentum fluxes in the flow are normally expected to

¹ Values for the cosmological parameters of $H_0 = 70 \text{ km s}^{-1} \text{ Mpc}^{-1}$, $\Omega_{m0} = 0.3$, and $\Omega_{\Lambda0} = 0.7$ are adopted throughout this review.

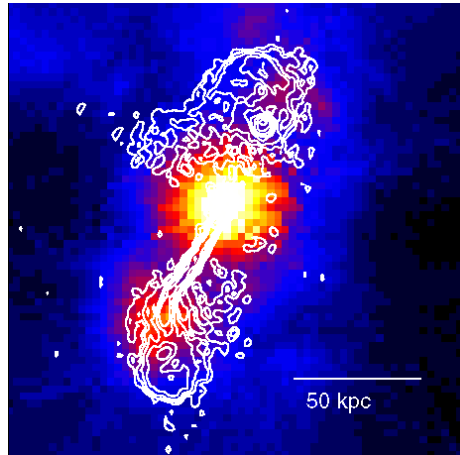


Fig. 2 The $z = 0.458$ FR II radio galaxy 3C 200. A smoothed 0.3-5 keV *Chandra* X-ray image of ~ 14.7 ks livetime is shown with radio contours from a 4.86 GHz *VLA* radio map [135] (beam size $0.33'' \times 0.33''$). Both nuclear [11] and extended X-ray emission are detected. A rough correspondence of some of the extended X-ray emission with the radio lobes has resulted in the claim for inverse-Compton scattering of the CMB by electrons in the lobes [55], but most of the extended emission over larger scales is now attributed to cluster gas [12].

be sufficient to drive a bow shock into the ambient medium. The ambient gas, heated as it crosses the shock, forces old jet material that has passed through the hotspots into edge-brightened cocoons. FR II jets are thus low-efficiency radiators but efficient conveyors of energy to large distances. They are often hundreds of kpc in length (particularly when deprojected for their angles to the line of sight), crossing many scale heights of the external medium from relatively dense gas in a galaxy core to outer group or cluster regions where the external density and pressure are orders of magnitude lower. State-of-the-art three-dimensional magneto-hydrodynamical simulations that incorporate particle transport and shock acceleration do well at reproducing the essential characteristics of synchrotron emission from such a source, and suggest that the shock and magnetic-field structures of the hotspots and lobes are extraordinarily complex and unsteady [201; 202].

1.4 Lifetimes and duty cycles

Individual FRI and FR II radio galaxies are thought to live for at most some tens of millions of years [e.g., 140; 118]. Age estimates are based on measuring curvature in the radio spectra caused by radiative energy losses of the higher-energy electrons over the lifetime of the sources [e.g., 3]. In contrast to the relative youth of observed radio structures, present-day clusters were already forming in the young Universe. Ideas that radio sources have an important rôle in heating cluster gas (see §7) then require a correct balance between the duty-cycle of repeated radio activity and heating efficiency as a function of jet luminosity. The duty cycle can be probed by searching for evidence of repeated activity from individual sources. Radio sources classified as GHz-Peaked Spectrum (GPS) or Compact Steep Spec-

trum (CSS) are small and believed to be either young or have their growth stunted by the external medium [151], and source statistics suggest that if they evolve to kpc-scale sizes they must dim while so doing [162]. VLBI kinematic studies provide convincing evidence that sources in the Compact Symmetric Object (CSO) subset, at least, are young, with current ages less than 10^4 years [52]. The fact that it is relatively uncommon to see GPS sources with extended radio emission that may be a relic of previous activity has been used to argue that periods between sustained activity are generally at least ten times longer than the radiative lifetime of the radio emission from the earlier activity [190]. This is consistent with a time between episodes of activity in FRIs of between about 5×10^8 and 10^9 years that is estimated using optical- and radio-catalog cross correlations coupled with an average source lifetime of about 1.5×10^7 years from modelling projected source lengths [18]. Of course, within the lifetime of an individual radio source there might be shorter-term interruptions or variations of activity (see §8.1).

2 Are the radio structures in a state of minimum energy?

2.1 Calculation of the minimum-energy field

The magnetic field strength and particle spectrum are important for jet physics as they define the internal pressure. The level of synchrotron radiation depends on the magnetic-field strength and the number of relativistic electrons and positrons, but these quantities are inseparable based on the observed synchrotron radiation alone. To progress further it is usual to assume that the source is radiating such that its combined energy in relativistic particles and magnetic field is a minimum [35]. In this situation the energy in the magnetic field is $\sim 3/4$ of the energy in the relativistic particles, and so this is similar to the condition in which the two are equal and the source is in ‘equipartition’. A change in any direction of the ratio of energy density in particles to magnetic field increases the total energy and pressure in the emitting plasma.

The minimum-energy magnetic field for a power-law spectrum of electrons producing radiation of a measured flux density at a particular frequency can be calculated analytically [e.g., 220], and for more complicated spectra the results can be obtained via numerical integration. Physical insight can be gained by considering a power-law spectrum where electrons give rise to a synchrotron luminosity, L_ν , at a given frequency ν of the form

$$L_\nu \propto \nu^{-\alpha}. \quad (1)$$

It is now normally thought preferable to define the spectral limits via a minimum and maximum Lorentz factor for the electrons in the source frame, γ_{\min} and γ_{\max} , [e.g., 220], rather than as synchrotron frequencies in the observer’s frame [e.g., 147], since the former is related to acceleration processes and has the potential for being chosen on a physical basis. Except in the special case of $\alpha = 0.5$, the minimum-energy magnetic field strength, B_{me} , is given by

$$B_{\text{me}} = \left[\frac{(\alpha + 1)C_1 (1 + K)}{2C_2} \frac{(1 + K)}{\eta V} L_\nu \nu^\alpha \frac{(\gamma_{\max}^{1-2\alpha} - \gamma_{\min}^{1-2\alpha})}{(1 - 2\alpha)} \right]^{1/(\alpha+3)}, \quad (2)$$

where V is the source volume, and C_1 and C_2 are combinations of fundamental physical constants and functions of α given by synchrotron theory [for details see 220]. Following the notation of [147], K is the ratio of energy in other relativistic particles to that in the electron and positron component, and η is the fraction of the volume filled by particles and fields (the so-called filling factor). The true minimum energy is when the only relativistic particles are radiating leptons, and the volume is completely and uniformly filled with radiating particles and fields. Some authors consistently use these assumptions when calculating B_{me} . If $K > 0$ or $\eta < 1$ then B_{me} is increased. Results for B_{me} are more strongly dependent on γ_{min} than γ_{max} , since $\alpha > 0.5$ for most observed radio spectra.

Relativistic beaming of a source affects B_{me} (as considered later in §3.2). Since there is inevitably uncertainty in the value of beaming parameters, B_{me} is best measured in components for which bulk relativistic motion is believed to be small or negligible. Of course, even in the absence of relativistic beaming, the angle to the line of sight, θ , enters into the calculation via a correction from projected linear size into true source volume, V . Typical values found for B_{me} in radio lobes and hotspots are 2–200 μGauss (0.2–20 nT) [e.g., 119], although a hotspot field as large as 3000 μGauss has been measured [91].

Figure 3 shows the dependence of B_{me} on γ_{min} , K , η , and θ , separately for electrons giving rise to synchrotron spectra with $\alpha = 0.6$ and $\alpha = 1.1$. The former slope is as expected from electrons undergoing highly relativistic shock acceleration [1], and the latter where energy losses have steepened the spectrum. The curves show that B_{me} changes rather little (within factors of at most a few) for rather large changes in the input assumptions.

2.2 Using X-rays to test minimum energy

The minimum-energy assumption can be tested by combining measurements of synchrotron and inverse-Compton emission from the same electron population. If the inverse Compton process is responsible for most of the X-ray radiation that is measured, and the properties of the photon field are known, the X-ray flux density is proportional merely to the normalization of the electron spectrum, κ , if the usual power-law form

$$N_e^{(\text{rel})} = \kappa \gamma^{-p} \quad (\gamma_{\text{min}} \leq \gamma \leq \gamma_{\text{max}}) \quad (3)$$

is assumed, where $N_e^{(\text{rel})}$ is the number of relativistic electrons per unit γ . The upscattered photons might be the CMB, whose properties are well known. Alternatively they could be the radio synchrotron radiation itself, in the process known as synchrotron self-Compton (SSC), or photons from the active nucleus, particularly at infrared through ultraviolet frequencies. Since the available photons range in frequency, so too do the energies of electrons responsible for scattering them into the X-ray, and these are rarely the same electrons for which the magnetic field is probed through synchrotron radiation. Nevertheless, it is usual to assume that the magnetic field, photons, and relativistic electrons are co-located, with the synchrotron photon density proportional to $\kappa B^{1+\alpha}$. Here α is defined as in Equation 1, and theory gives $\alpha = (p - 1)/2$. The combination of synchrotron (radio)

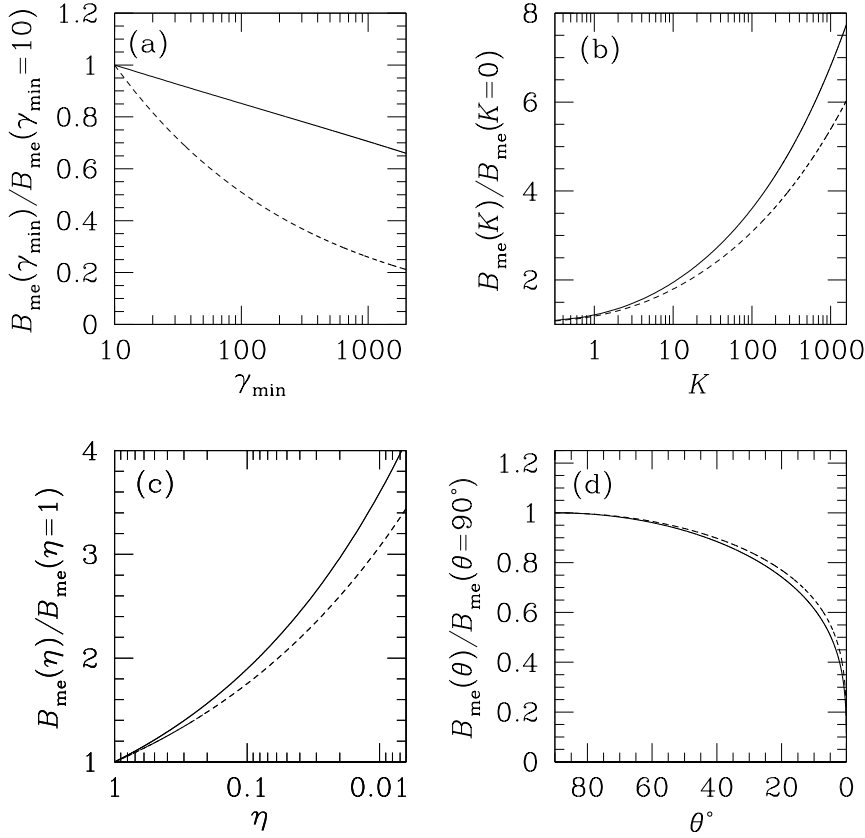


Fig. 3 Effect on the calculated minimum-energy magnetic field if a parameter value is varied from its nominal value (left-hand-side of plot). Results are for a power-law electron spectrum, extending from Lorentz factor γ_{min} to $\gamma_{\text{max}} = 10^5$, that gives rise to a synchrotron spectrum $S_\nu \propto \nu^{-\alpha}$ with $\alpha = 0.6$ (solid lines) and $\alpha = 1.1$ (dashed lines). (a): increasing γ_{min} from a value of 10. (b): increasing the ratio of energy in other particles to that in electrons, K , from a value of zero. (c): decreasing the filling factor, η , from a value of 1. (d) decreasing the angle to the line of sight, and thus increasing the source volume from the projected size at $\theta = 90^\circ$.

flux density and inverse Compton (X-ray) flux density then allows a value for the magnetic field strength, B_{SiC} , to be inferred and compared with B_{me} .

Since the modelling requires that the volume and any bulk motion of the emitting plasma be known, the best locations for testing minimum energy are the radio hotspots, which are relatively bright and compact, and are thought to arise from sub-relativistic flows at jet termination [but see 80], and old radio lobes where the plasma may be relatively relaxed. There is no reason to expect dynamical structures to be at minimum energy.

It was anticipated that *Chandra* and *XMM-Newton* would make important advances in tests of minimum energy, since already with *ROSAT* and *ASCA* there were convincing detections of inverse Compton X-ray emission from the hotspots

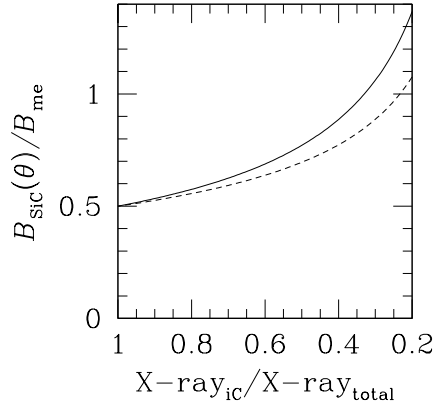


Fig. 4 The amount by which the fraction of the total X-ray flux density attributable to inverse Compton radiation, $X\text{-ray}_{\text{ic}}/X\text{-ray}_{\text{total}}$, would have to be reduced for a result of $B_{\text{SiC}}/B_{\text{me}} = 0.5$ to be increased. Solid and dashed curves are for $\alpha = 0.6$ and $\alpha = 1.1$, respectively.

and lobes of a handful of sources [e.g., 101; 76; 195], and pioneering work on the hotspots of Cygnus A had found good agreement with minimum energy [101]. *Chandra* and *XMM-Newton* have allowed such tests to be made on a significant number of lobes and hotspots, with results generally finding magnetic field strengths within a factor of a few of their minimum energy (equipartition) values for $K = 0$ and $\eta = 1$ [e.g., 95; 33; 110; 51; 30; 10; 54; 148]. A study of ~ 40 hotspot X-ray detections concludes that the most luminous hotspots tend to be in good agreement with minimum-energy magnetic fields, whereas in less-luminous sources the interpretation is complicated by an additional synchrotron component of X-ray emission [98]. Considerable complexity of structure is seen where hotspots are close enough for X-ray images to have kpc-scale or better resolution [e.g., 126].

For radio lobes, the largest systematic study where it is assumed that all the X-ray emission is inverse Compton radiation is of 33 FR II lobes, and finds $0.3 < B_{\text{SiC}}/B_{\text{me}} < 1.3$ [55]. Since the asymmetry is on the side of $B_{\text{SiC}} < B_{\text{me}}$, it is important to recognize that the analysis may not have accurately taken into account contributions to the lobe X-ray emission from cluster gas, now commonly detected away from the lobe regions in FR II radio galaxies [12, and see Fig. 2]. However, as seen in Figure 4, the lobe X-ray emission from cluster gas would have to be far brighter than that from inverse Compton scattering to cause $B_{\text{SiC}}/B_{\text{me}}$ to increase significantly (e.g., from 0.5 to 1.0), and this is incompatible with the observation that lobes stand out in X-rays as compared with adjacent regions.

Better agreement between B_{SiC} and B_{me} would be achieved if B_{me} has been overestimated. Figure 3 shows that decreasing the filling factor or including relativistic protons that energetically dominate the electrons have the opposite effect. A decrease in B_{me} is found if the source has been assumed to be in the plane of the sky whereas it is really at a small angle, with the structures having more volume. However, the small angles required to make an appreciable difference would be inconsistent with random sampling. More promising would be if γ_{min}

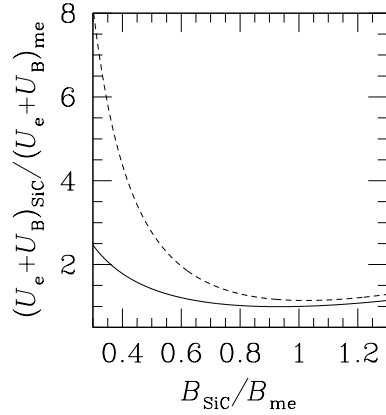


Fig. 5 The ratio of total energy in electrons and magnetic field, computed from combined X-ray inverse Compton and radio synchrotron measurements, to that calculated for minimum energy, for the range of $B_{\text{SIC}}/B_{\text{me}}$ typically observed. Solid and dashed curves are for $\alpha = 0.6$ and $\alpha = 1.1$, respectively.

were higher than typically assumed, as stressed by [27] who claim evidence for a value of γ_{min} as high as $\sim 10^4$ in the hotspot of one FR II radio galaxy, with a lower value of $\gamma_{\text{min}} \sim 10^3$ in the lobes as a result of adiabatic expansion. This is in line with earlier measurements of spectral flattening at low radio frequencies in hotspot spectra, suggestive of values of γ_{min} no lower than a few hundred [e.g., 133; 41]. Why there might be such a γ_{min} in a hotspot is discussed by [91].

It is important to stress that finding $B_{\text{SIC}}/B_{\text{me}}$ within a factor of a few of unity does not allow strong constraints to be placed on physical parameters. As shown in Figure 3, large changes in input parameters do not change B_{me} , and thus $B_{\text{SIC}}/B_{\text{me}}$, by a large amount. It is often pointed out that if the magnetic-field strength is a factor of a few below B_{me} , the energy in relativistic electrons must dominate the magnetic-field energy by orders of magnitude. While this is relevant for understanding the state of the plasma, does this really matter from the point of view of source energetics? The increase in combined electron and magnetic-field energy over the minimum energy is relatively modest as long as the electron spectrum is not very steep and the field strength is no less than about a third of B_{me} (Fig. 5).

In any case, it is clear that application of minimum energy over large regions is an oversimplification. Three-dimensional magneto-hydrodynamical simulations that incorporate particle transport and shock acceleration [201; 202] find much substructure of particle distributions and fields within the volumes typically integrated over observationally. Complexity on a coarser scale is seen in some observations [e.g., 110; 148].

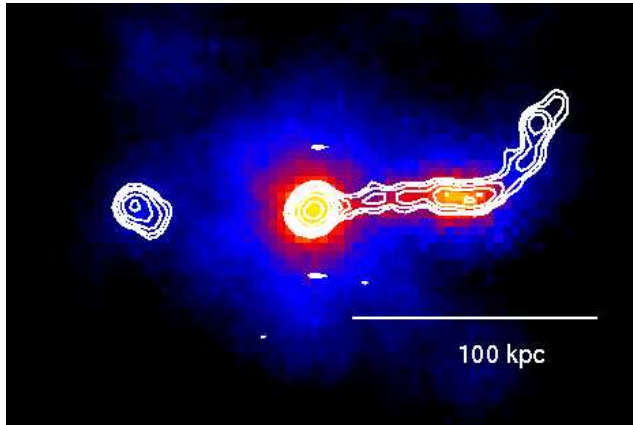


Fig. 6 The $z = 0.651$ quasar PKS 0637-752, using data from [177]. The plot shows a smoothed *Chandra* X-ray image of ~ 35 ks exposure with radio contours from an 8.64 GHz ATCA radio map (beam size $0.96'' \times 0.81''$). X-ray emission is detected from the nucleus and from the western radio jet before it bends north. The bright jet region $7.8''$ west of the nucleus is known as Knot WK7.8.

3 Do powerful large-scale jets have fast spinal speeds?

3.1 The impetus from PKS 0637-752

Chandra is central to the current debate concerning jet speed in the powerful radio jets of quasars. The work was kick-started unexpectedly. Observing quasars was not initially a high scientific priority for *Chandra*, as it was recognized that the cores were bright, and the likelihood of multiple photons arriving between CCD readouts was high, leading to distorted spectral measurements (so called ‘pileup’). It was thus fortuitous that a radio-loud quasar was the chosen target for in-flight focus calibration, since this led to the detection of resolved jet emission from the $z = 0.651$ quasar PKS 0637-752 [177; 45, and see Fig. 6].

Several possible origins for PKS 0637-752’s jet X-rays were considered. The level of optical emission was too low to explain the X-rays as the synchrotron radiation from a single population of electrons, and SSC was disfavoured as it would require strong dominance of the energy in relativistic electrons over that in magnetic field, giving a total energy in particles and field that is ~ 1000 times that given by minimum energy [177]. A more promising explanation allowed the jet to be at minimum energy but required it to have fast bulk motion (a Lorentz factor of $\Gamma \sim 20$ at $\theta \sim 5^\circ$ to the line of sight), in which case it would see boosted CMB in its rest frame and emit beamed X-rays in the observer’s frame [197; 44]. Although such a speed and angle are consistent with VLBI measurements on pc scales [139], the fast speed must persist up to hundreds of kpc from the core (after projection is taken into account) for the X-rays to be produced by this mechanism, which I will call “beamed iC-CMB”. This explanation ran counter to the common wisdom of the time, based on radio data, that the bulk relativistic speed of quasar jets on the large scale is $\Gamma \sim 2$ [e.g., 31; 208]. To overcome the contradiction, it was suggested that quasar jets have a fast-moving central spine responsible for

the observed X-rays, and a slower-moving outer region that emits the bulk of the observed radio emission [44]. This follows the same pattern as the transverse velocity structures, conjectured for FRI jets, that are thought to result from the entrainment of external material (see §4).

3.2 The dependence of beamed iC-CMB on beaming factors and redshift

In modelling beamed iC-CMB emission, most authors use the approximation that CMB photons, isotropic in the observer's frame, are scattered into directions in the jet frame that are parallel to the instantaneous velocity vectors of the scattering electrons [e.g., 58; 102]. This has been shown to be an excellent approximation for calculating the X-ray emissivity as long as the jet's bulk motion has Lorentz factor $\Gamma \geq 2$ [59], which is, in any case, required for the mechanism to be effective at producing strong X-ray fluxes. The basic physics of the formalism is particularly clearly presented in [58], and here those formulae are presented in a slightly different form which is independent of the system of units.

We consider a source travelling at speed βc and bulk Lorentz factor Γ towards the observer at an angle θ to the line of sight, so that the bulk relativistic Doppler factor, δ , is given by

$$\delta = \frac{1}{\Gamma(1 - \beta \cos \theta)}. \quad (4)$$

An electron of Lorentz factor γ will scatter a CMB photon that has a characteristic frequency today of ν_{CMB} to an observed frequency, ν , given by

$$\nu = \nu_{\text{CMB}} \gamma^2 \frac{\delta^2(1 + \cos \theta)}{(1 + \beta)}, \quad (5)$$

where the spectral redistribution function is approximated as a delta function [equation (7) of 58, written in the notation of this paper]. A delta-function approximation is also used for the synchrotron spectral distribution function such that an electron of Lorentz factor γ radiates at frequency

$$\nu = \gamma^2 \nu_g, \quad (6)$$

where ν_g is the non-relativistic electron gyrofrequency, which is proportional to the magnetic field strength, B . Written in SI units, $\nu_g = eB/2\pi m_e \approx 30B$ GHz, where B is in units of Tesla. For a CMB that is monochromatic at a frequency of ν_{CMB} at redshift equal to zero, then the ratio of inverse Compton to synchrotron flux density at a fixed frequency in the observer's frame is simply given by

$$\frac{S_{\text{iC-CMB}}}{S_{\text{syn}}} = \frac{3}{4} \delta^{1+\alpha} (1+z)^{3+\alpha} \left(\frac{1 + \cos \theta}{1 + \beta} \right)^{1+\alpha} \frac{u_{\text{CMB}}}{u_B} \left(\frac{\nu_{\text{CMB}}}{\nu_g} \right)^{\alpha-1}, \quad (7)$$

where u_{CMB} is the energy-density of the CMB at a redshift of zero and u_B is the energy density in the magnetic field in the rest-frame of the jet. Noting that $u_B \propto B_{\text{int}}^2$ and $\nu_g \propto B_{\text{int}}$, where B_{int} is the intrinsic magnetic-field strength in the rest-frame of the jet,

$$\frac{S_{\text{iC-CMB}}}{S_{\text{syn}}} \propto \frac{\delta^{1+\alpha}}{B_{\text{int}}^{1+\alpha}} (1+z)^{3+\alpha} \left(\frac{1+\cos\theta}{1+\beta} \right)^{1+\alpha}. \quad (8)$$

If the modelling assumes minimum energy in relativistic particles and fields, then Equation 2 can be used. The luminosity density can be written in terms of the observable synchrotron flux density using

$$L_{\nu} \delta^{(3+\alpha)} = (1+z)^{\alpha-1} S_{\nu} 4\pi D_{\text{L}}^2, \quad (9)$$

where D_{L} is the luminosity distance. The volume of a radio source can be specified in terms of its angular component sizes, θ_x , θ_y and path length through the source, d , as

$$V = \theta_x \theta_y d D_{\text{L}}^2 / (1+z)^4. \quad (10)$$

Substituting for L_{ν} and V (Equations 9 and 10) in Equation 2 then gives

$$B_{\text{me}} = \left[\frac{(\alpha+1)C_1}{2C_2} \frac{(1+K)}{\eta \theta_x \theta_y d} 4\pi \frac{S_{\nu}}{\delta^{(3+\alpha)}} v^{\alpha} (1+z)^{3+\alpha} \frac{(\gamma_{\text{max}}^{1-2\alpha} - \gamma_{\text{min}}^{1-2\alpha})}{(1-2\alpha)} \right]^{1/(\alpha+3)}, \quad (11)$$

i.e.,

$$B_{\text{me}} \propto \frac{(1+z)}{\delta}. \quad (12)$$

Substituting for $B_{\text{int}} = B_{\text{me}}$ in Equation 8 gives

$$\frac{S_{\text{iC-CMB}}}{S_{\text{syn}}} \propto \delta^{2+2\alpha} (1+z)^2 \left(\frac{1+\cos\theta}{1+\beta} \right)^{1+\alpha}. \quad (13)$$

Equation 9 (and thus Equations 11, 12 and 13) applies to a spherical blob in which $S_{\text{syn}} \propto \delta^{3+\alpha}$: for a continuous jet where $S_{\text{syn}} \propto \delta^{2+\alpha}$, $B_{\text{me}} \propto 1/\delta^{(2+\alpha)/(3+\alpha)}$, and Equation 13 has a slightly more complicated dependence on δ . Also, Equation 10 adopts the assumption that the pathlength through the jet is independent of redshift. Alternative assumptions could be adopted, modifying the redshift dependencies in Equations 11, 12 and 13.

3.3 How is the beamed iC-CMB model faring under scrutiny?

It was obvious that there were important consequences if the beamed iC-CMB interpretation of the X-ray emission from the resolved jet of PKS 0637-752 is correct, and holds for other quasar jets. In particular, increasing Γ from the previously accepted value of ~ 2 to $\Gamma \sim 20$ means increasing the jet power by a factor of ~ 100 , or more if cold ions are an important contributor to the jet composition [see appendix B of 178].

Programs targeting the resolved radio jets of core-dominated quasars with *Chandra* followed the work on PKS 0637-752 [170; 171; 141]. The detection success rate of roughly 50 per cent in relatively short exposures made it clear

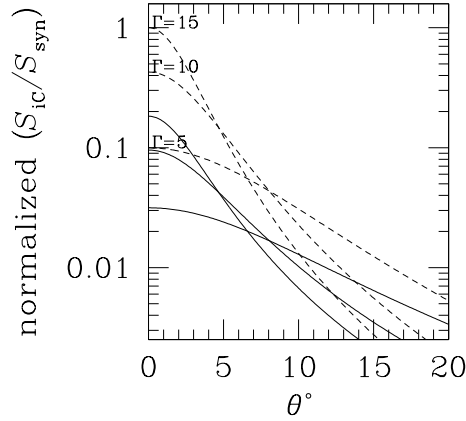


Fig. 7 Normalized ratio of inverse Compton to synchrotron flux density for a fixed intrinsic magnetic field strength for different jet angles to the line of sight. The normalization is to the value for a jet with a Lorentz factor of 15 and $\alpha=1.1$ at 0° to the line of sight. Solid and dashed curves are for $\alpha = 0.6$ and $\alpha = 1.1$, respectively. Each set has curves for $\Gamma = 15$, $\Gamma = 10$, and $\Gamma = 5$, in descending order at $\theta = 0^\circ$. Based on Equation 8.

that PKS 0637-752 is not an outlier. Longer *Chandra* observations were made of some of the X-ray brightest and morphologically most interesting sources [e.g., 142; 169; 181; 182; 183; 115; 116; 178; 180; 179; 200]. The combination of surveys and long pointed observations have made it possible to look critically at the application of the beamed iC-CMB model to these sources.

The high X-ray detection rate of quasar jets in short exposures is notable. In most *Chandra* observations of FR II radio galaxies at similar redshifts to the quasars, the jets (as opposed to the terminal hotspots) are not detected [e.g., 218; 12]. This can be understood in the framework of quasar/radio-galaxy unification with reference to Figure 7 (based on Equation 8) which shows that for jets that are intrinsically the same, the ratio of beamed-iC to synchrotron radiation strongly decreases with increasing jet angle to the line of sight. The observed quasar X-ray jet emission is normally one-sided and on the same side as the brighter radio jet, in support of relativistic beaming. Where two-sided X-ray emission has been seen, explanations can be found which are not in violation of fast jet speeds [e.g. 71; 120].

In general the jets contain multiple knots that can be fitted independently to the beamed iC-CMB model with minimum-energy magnetic field strengths of order 10–20 μG (1–2 nT) [e.g., 178]. Note, however, that there are insufficient observational constraints to fit the two free parameters of angle to the line of sight and bulk Lorentz factor separately, and an assumption must be made on one of these parameters. It has been common to assume $\sin \theta = 1/\Gamma$ (i.e., $\delta = \Gamma$), although this is not particularly sensible for sources where multiple knots in the same source give different values for Γ , since it can lead to a jet that bends more erratically than makes physical sense. In some cases the results can be shown to agree with the

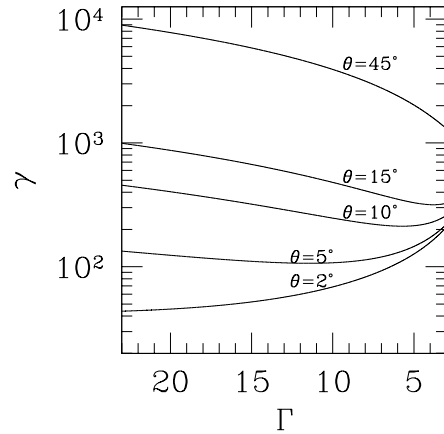


Fig. 8 Mean Lorentz factor, γ , of electrons which scatter CMB photons near the black-body peak to X-ray photons of 1 keV. Results are shown for an emission region at selected angles to the line of sight over a range of bulk Lorentz factor, Γ . Based on Equation 5.

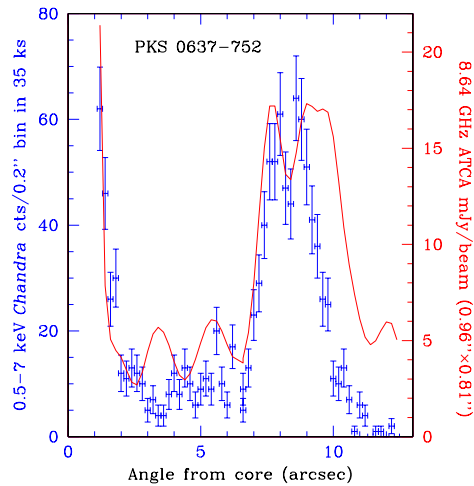


Fig. 9 The X-ray and radio profiles down the jet of PKS 0637-752 (see Fig 6). The X-ray intensity drops before the radio at large jet angles. $1''$ corresponds to a projected linear distance of 6.93 kpc.

estimates of speed and power from simple models for the pc-scale emission [e.g., 116; 200, and see §8.4], although with rather large uncertainties.

There is, however, a major difficulty with the beamed iC-CMB interpretation that arises from a detailed comparison between radio and X-ray emission. Figure 8 (based on Equation 5) shows the mean Lorentz factor of electrons that scatter photons from the peak of the CMB spectrum into the X-ray at 1 keV, for various jet

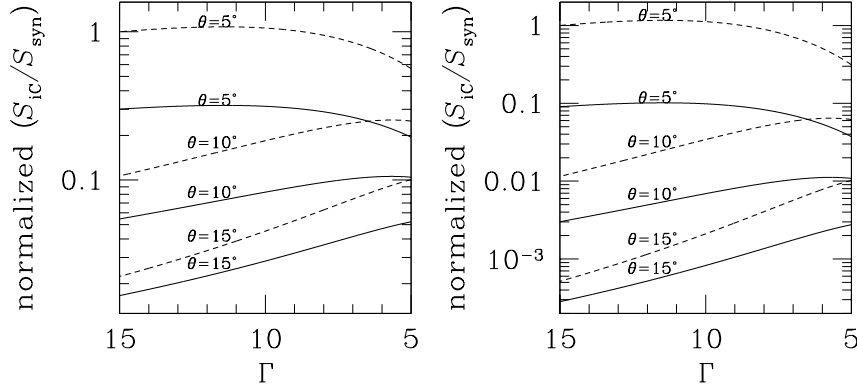


Fig. 10 Normalized ratio of inverse Compton to synchrotron flux density for a fixed jet angle to the line of sight with decreasing Lorentz factor, Γ . Left: with fixed intrinsic magnetic field. Right: with minimum-energy magnetic field. In each panel separately the curves are normalized to the value of $S_{\text{IC}}/S_{\text{syn}}$ for a jet with a Lorentz factor of 15, $\alpha=1.1$, at 5° to the line of sight. Solid and dashed curves are for $\alpha = 0.6$ and $\alpha = 1.1$, respectively. Each set has curves for $\theta = 5^\circ$, $\theta = 10^\circ$, and $\theta = 15^\circ$, in descending value on the y-axis at $\Gamma = 15$.

bulk Lorentz factors and angles to the line of sight. The synchrotron emission from these electrons will be at a peak frequency of $\approx \gamma^2 \nu_g \approx 30\gamma^2 B$ GHz, where ν_g is the gyrofrequency and B is magnetic field strength in Tesla. For a typical field of 2 nT, the radio synchrotron emission from these electrons is at 0.3 MHz if $\gamma = 100$, or 20 MHz if $\gamma = 10^3$, both below the observable radio band. Under the beamed iC-CMB model, which requires small angle to the line of sight, θ , to be effective, the X-ray emission thus arises from lower-energy electrons than the radio emission. These electrons have long synchrotron energy-loss lifetimes. However, observations sometimes show X-ray emission that weakens relative to the radio towards the downstream regions of the jets and in some cases in individual knots, indicating that the population of low-energy electrons is being depleted more rapidly than the population of high-energy electrons, contrary to expectations based on radiation losses. This was seen in PKS 0637-752 [177; 45, and see Fig. 9], and such behaviour is also seen strikingly in several other sources including 3C 273 [142; 169], quasar 0827+243 [115], PKS 1127-145 [181] and PKS 1136-135 [172]. Various suggestions have been made to overcome the problem within the framework of the beamed iC-CMB model, but none is uniformly regarded as satisfactory.

It has been suggested that strong clumping in the jets may resolve the problem through adiabatic energy losses [198]. However, it is not clear that the beamed iC-CMB mechanism is then required, since such clumping would increase the SSC yield for a slow jet at minimum energy [177]. Alternatively, it has been suggested that jet deceleration is important, perhaps through entrainment of external gas [e.g., 81; 172; 199]. A problem with this as a general solution is that, as shown in Figure 10 (based on Equations 8 and 13), the ratio of inverse Compton to synchrotron emission only falls for a decelerating jet over particular ranges of bulk Lorentz factor for jets at an angle of less than about 5° to the line of sight.

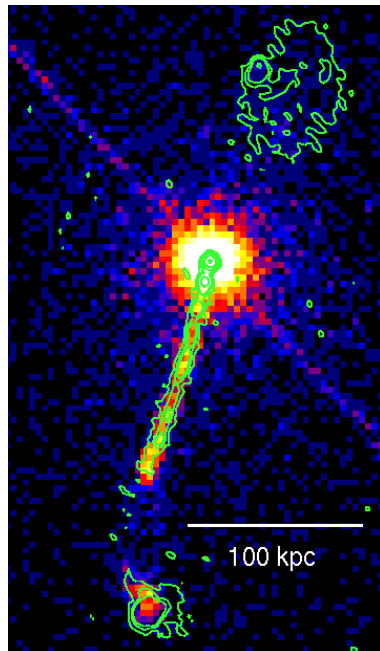


Fig. 11 The $z = 0.72$ quasar 4C19.44, using data from [179]. The plot shows an unsmoothed *Chandra* X-ray image of ~ 189.4 ks exposure with radio contours from a 4.86 GHz *VLA* radio map (beam size $0.47'' \times 0.43''$). X-ray emission is detected from the nucleus, the southern radio jet, the northern hotspot and southern radio lobe. The excess X-ray counts in a line running NE-SW centred on the nucleus are a frame-readout artifact.

This means that any source for which the X-ray drops off faster than the radio with downstream distance would need to be at particularly small angle to the line of sight or rather slow (but see [81] for a more detailed treatment that includes compression of the magnetic field and thus relative amplification of the radio synchrotron emission downstream). Jet deceleration is potentially testable through looking at the X-ray and radio profiles of source samples.

A point in favour of the beamed iC-CMB explanation is that the particularly straight knotty jet in the quasar 4C 19.44 shows one of the most uniform X-ray to radio ratios over almost a dozen discrete knots in its straightest section [179, and see Fig. 11]. In contrast to PKS 0637-752, the radio drops more rapidly than the X-ray at the end of the straight, well-collimated jet beyond about $15''$ from the nucleus (Fig. 12). This might suggest that drops in the level of X-ray to radio emission along other jets are the result of the jets bending out of the line of sight. Since quasar jets are selected for observation based partly on their core radio emission, any bending downstream is more likely in a direction away from the line of sight than towards it. A large change in jet angle could easily produce the typical decreases in X-ray to radio ratio (a factor of a few to about 10; compare with Fig. 7). However, it is difficult to understand how a real change in angle of a $\Gamma \sim 20$ flow by more than about a degree could occur without severe jet decolli-

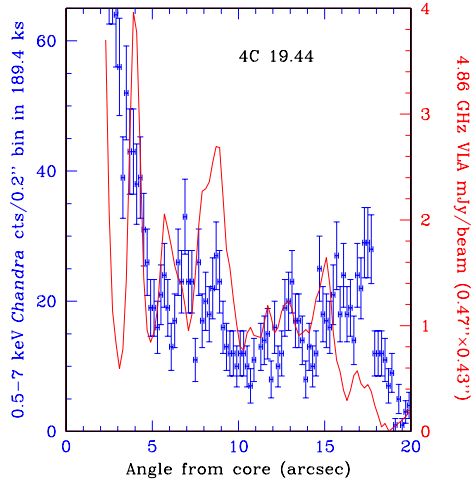


Fig. 12 The X-ray and radio profiles down the jet of 4C 19.44 (see Fig. 11). In contrast to PKS 0637-752 (Fig. 9), the radio intensity drops before the X-ray at large jet angles. $1''$ corresponds to a projected linear distance of 7.23 kpc.

mation². As apparent from Figure 7, more than a factor of about two decrease in X-ray to radio ratio is then not expected from bending alone.

A test that the beamed iC-CMB explanation must pass concerns the redshift dependency. The increase in CMB energy density with redshift means that the X-ray to radio ratio should increase with redshift by a factor of something like $(1+z)^2$ (Equation 13: the precise dependence on redshift depends on assumptions concerning minimum energy and whether or not the path length through the source is redshift dependent). Such a redshift effect is not ruled out [141] although a larger sample is needed for a more definitive test.

3.4 Synchrotron emission as an alternative

The fast jet speed required for the beamed iC-CMB explanation of quasar X-ray emission disappears if an alternative explanation can be found for the X-rays. It is then natural to invoke synchrotron radiation, the mechanism producing the X-rays in low-power FRI jets (see §5.1). However, whereas for FRI jets the SED can normally be modelled with a broken power-law spectrum from the radio, through the optical to the X-ray [e.g., 29; 96; 21], PKS 0637-752 has too little optical emission to allow this, and a separate population of electrons with an anomalously high low-energy cutoff would be required [177]. Figure 13 compares the spectral distribution of the FRI radio galaxy M 87, where a broken-power-law synchrotron components fits well, with that of the FRII quasar PKS 0637-752.

Most of the several tens of current quasar X-ray jet detections were found through targeted *Chandra* programs to observe bright, prominent, one-sided radio

² Large changes in jet angle in projection are observed in many sources, but Figure 7 relates to the true jet angle to the line of sight.

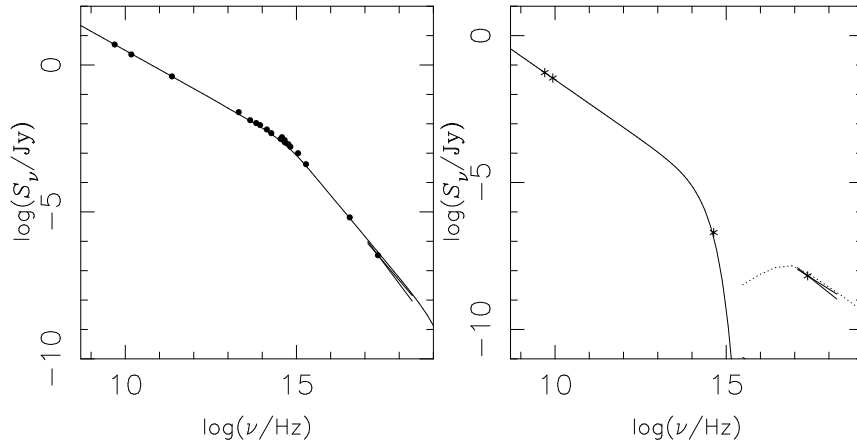


Fig. 13 Spectral distributions from the radio to X-ray. Left: The integrated emission from Knots A, B and C of M 87, using data from [28] and [13], fits a broken power law synchrotron spectrum, although the change of 1.5 in electron spectral slope is greater than expected from a simple model for synchrotron energy losses. Right: A broken power-law spectrum does not fit through the emission from Knot WK7.8 of PKS 0637-752 (taken from [45]) although a synchrotron component with an exponential cutoff and either a beamed iC-CMB component or a separate synchrotron component with an anomalously high low-energy cutoff can be made to fit the data.

jets. In most cases there was no pre-existing reported optical jet detection, but there has been reasonable success from follow-up work. The level of such optical detections often lies below an interpolation between the radio and X-ray spectra, supporting the idea that synchrotron emission from a single power-law distribution of electrons is not responsible for all the emission [e.g., 171].

However, the conclusion regarding synchrotron emission is not quite as clear cut, since a single-component electron spectrum will harden at high energies if inverse-Compton losses are also important (since this loss process is less efficient in the Klein-Nishina regime), and the consequent spectral hardening in the synchrotron spectrum might then better match observations [60].

As long as electrons can be accelerated to high energy (and they can be in FRIs) they will produce synchrotron radiation at some level. Radio galaxies are at large angle to the line of sight and any iC-CMB emission will be beamed out of the line of sight of the observer (an extension of Fig. 7 to large angle shows that, even for the most optimistic case, the ratio of iC-CMB to synchrotron emission drops three orders of magnitude between $\theta = 0$ and $\theta = 80^\circ$). Indeed, synchrotron X-ray emission from knots in the radio jets of nearby FRII radio galaxies is reported [e.g., 212; 219; 125; 120]. When optical detections are also available, the energy distributions [125; 219] are of similar simple form to those in FRIs (see Fig. 14), not requiring the complex electron spectral forms generally needed to explain quasar X-ray emission as synchrotron radiation. Spatial offsets reminiscent of those seen in FRIs and which are presumably a feature of the particle acceleration processes (see §5.2) are also seen [219; 120].

It remains uncertain as to whether or not in quasars it is necessary to explain the jet X-ray emission as the synchrotron output of a distorted electron spectrum

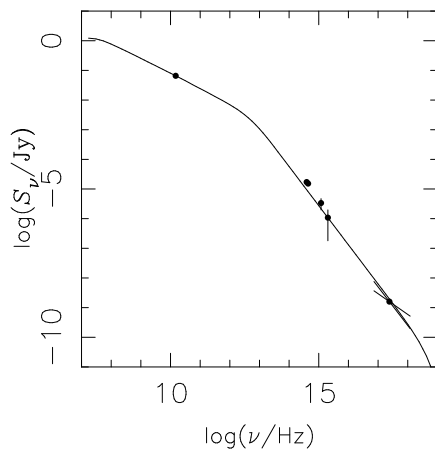


Fig. 14 The spectrum from the radio to X-ray for the knot in the FRII radio galaxy 3C 346 (see Fig. 16) fits a broken-power-law synchrotron model.

[60] or from separate populations of electrons [e.g., 7], as an alternative to the beamed iC-CMB model. In the case of 3C 273, the run of X-ray spectral slope down the jet rules out a simple beamed iC-CMB interpretation, but a two-zone iC-CMB model with a faster spine, although disfavoured, cannot be ruled out [112]. If a synchrotron interpretation is sought, similar, simple electron spectra in all jet regions do not fit observations [e.g., 166; 169; 142]. A two-zone model with faster spine has been proposed, where, unlike for beamed iC-CMB in which the X-rays are from the spine, the X-rays would arise from the shear layer through electron acceleration to very high energy [112].

It is important to understand the primary X-ray emission in quasar jets, and this remains an observational problem — more work on samples and further detailed, deep, multiwavelength observations of individual sources are needed. Predictions for yields at higher energies also differ according to the X-ray emission mechanism, and so there is a prospect that the new Fermi Gamma-ray Space Telescope will help in finding solutions [e.g., 60; 83]. Optical polarimetry is potentially a strong discriminant since, unlike for optical synchrotron emission, the optical emission should be essentially unpolarized if it is a lower-energy extension of X-ray emission that is produced via the beamed iC-CMB mechanism [e.g., 113; 203].

4 What keeps jets collimated?

X-ray measurements of the external medium support arguments that low-power FRI jets slow through entrainment of this gas.

For the few low-power radio galaxies with heavily studied, straight, radio jets and counterjets (and so lying relatively close to the plane of the sky and presumably in relatively relaxed environments), kinematic models have been constructed to fit the jet-counterjet asymmetry [131; 38; 39; 132]. Typically, the jets start fast (relativistic) and relatively faint with a small opening angle. Then they go through a flaring region where they steadily broaden and are typically bright both in ra-

dio and X-ray (Fig. 1), and finally the opening angle changes and the jet becomes fainter, particularly at X-ray energies [e.g., 221]. It is in this final region, beyond that shown for NGC 315 in Figure 1, that the jets are modelled as decelerating steadily as they collect mass from the external medium or stellar winds [122]. Buoyancy forces are then important for much of the flow further downstream, as the jets adjust to changes in the density of the external medium, causing deflections from straight-line motion.

In ongoing work, these kinematic models are being extended into dynamical models, based on conservation laws for mass, momentum, and energy [16], and are being tested for self consistency with the density and pressure of the external medium. For one source so far, 3C 31, excellent self consistency has been found [130]. This lends confidence to an understanding of the basic flow behaviour of these sources.

Deceleration via mass entrainment is consistent with a range of observational evidence at radio frequencies [129], and naturally leads to the outer parts of the jet (sheath) being decelerated before the inner (spine). Applied to more central regions, the consequence that emission from a slower sheath becomes relatively more important in jets at larger angle to the line of sight then resolves difficulties in models that unify BL Lac objects with FRI radio galaxies [e.g., 48].

It has been known since the *Einstein* and *ROSAT* X-ray observatories that the minimum pressure in low-power FRI jets (calculated without relativistic protons) is normally below that of the external X-ray-emitting medium [e.g., 149; 121; 77; 216]. The model for 3C 31 [130] demonstrates that entrainment of the external medium explains the jet dynamics in the deceleration region, and pressure balance can be achieved by adding relativistic protons (with neutrality preserved by balancing proton and electron number densities) or extending the electron spectrum to lower energies (if electron-positron charge balance is enforced). Recent work [56] has claimed a greater pressure imbalance in FRI jets that are more in contact with external gas (less in contact with the plumes or lobes of older jet plasma), and speculates that the pressure is balanced by heated entrained material, with an entrainment rate or a heating efficiency that is higher where jets are in greater direct contact with the X-ray-emitting atmosphere. This seems in conflict with the entrainment model for the quasar PKS 1136-135 in the context of the beamed iC-CMB model, where a standard model would have the jets heavily embedded in old lobe plasma and yet where the estimated entrainment rate is an order of magnitude higher than for 3C 31 [199].

While the X-ray-emitting interstellar or intergalactic medium can thus be controlling the flow where FRI jets are decelerating, and indeed where buoyancy forces or an excess of gas pressure dominate [e.g. 215; 222], FRI radio jets are highly overpressured in their inner regions close to the nucleus [e.g., 130]. Here the X-ray emission has yet to contribute in a significant way to the collimation debate.

The jets of FR II radio galaxies are not significantly in contact with the external medium for most of their length, so the external medium is unlikely to control jet collimation, although entrainment of external gas might be significant over their long propagation paths [199]. Current uncertainties in the jet X-ray emission mechanism, and thus the particle content and energy, make direct comparison of

the internal and external pressures difficult, except in the large-scale lobes if dynamical effects are ignored.

5 Where and how does particle acceleration occur?

5.1 The link with synchrotron X-ray emission

Chandra found X-ray synchrotron emission to be common in the resolved kpc-scale jets of FRI radio sources [217]. The X-ray jets are readily detected in sources covering the whole range of orientation in unified schemes. The several tens of detected sources range from beamed jets in BL Lac objects [21; 157; 173] to two-sided jets in radio galaxies [46; 97], with most X-ray jets corresponding to the brighter radio jet, [e.g., 217; 96; 104; 143; 68; 221]. Several of the observations have been targeted at sources already known to have optical jets, from ground-based work or *HST*. However, it's proved easier to detect X-ray jets in modest *Chandra* exposures than to detect optical jets in *HST* snapshot surveys, because of better contrast with galaxy emission in the X-ray band than in the optical [217].

Inverse Compton models for any reasonable photon field suggest an uncomfortably large departure from a minimum-energy magnetic field in most low-power X-ray jets [e.g., 96], although the beamed iC-CMB model is a contender for the emission from some BL Lac objects [e.g., 173]. Otherwise synchrotron emission from a single electron population, usually with a broken power law, is the model of choice to fit the radio, optical, and X-ray flux densities and the relatively steep X-ray spectra [e.g., 29; 96]. Given Equation 6, X-ray synchrotron radiation at 1 keV requires electrons of energy $\sim 10^{13}$ eV (Lorentz factor $\gamma \approx 2 \times 10^7$) if the magnetic field strength is of order 20 nT (200 μ G; the electron energy scales as $B^{-1/2}$). Averaging over pitch-angle distribution, the lifetime of synchrotron-emitting electrons is given by

$$\tau = \frac{3m_e c}{4\sigma_T u_B \gamma}, \quad (14)$$

where m_e is the electron mass, σ_T is the Thomson cross section, and u_B is the energy density in the magnetic field. We thus see that electrons emitting 1 keV synchrotron radiation in a 20 nT magnetic field have an energy-loss lifetime of about 30 years (lifetime scales as $B^{-3/2}$). The electrons must therefore be accelerated *in situ*, since their lifetimes against synchrotron losses are less than the minimum transport times from the active nuclei, or even from side to side across the jet. (This should not be the case if proton synchrotron radiation is important [2], since lifetime scales as $(m_p/m_e)^{5/2}$.) Particle acceleration is generally discussed for the cases of a particle interacting with a distributed population of plasma waves or magnetohydrodynamic turbulence, or shock acceleration [see e.g., 25; 66; 108; 5].

For electrons, particle acceleration and energy losses are in competition [e.g., 106], no more so than in hotspots of FRIIs [e.g., 34], which mark the termination points of the beam. Hotspots display considerable complexity in the X-ray, with synchrotron components seen in the less powerful sources indicating that TeV electrons are present [e.g., 98; 126]. It has been suggested that the low-energy

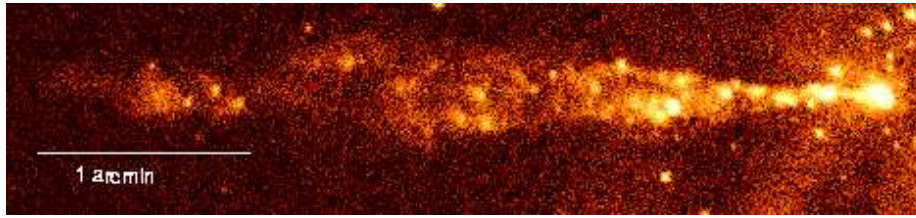


Fig. 15 A rotated image of a roughly 4.5 kpc (projected) length of the 0.8–3 keV X-ray jet of Cen A from combining six deep (~ 100 ks) *Chandra* exposures. Image taken from [223].

radio spectral-slope change seen in hotspots may mark a transition between electrons that are accelerated through electron-proton cyclotron resonance and those (at higher energy) that are simply undergoing shock acceleration [e.g., 192; 91]. If in FRIs the far-IR spectral break consistently maps electrons of a particular energy, it is possible that the break here is also more related to acceleration than loss processes [22].

Whether or not particle acceleration is required along the jets of quasars depends on the emission process at high energies. If the beamed iC-CMB model holds, then the electrons participating in radiation at wavelengths currently mapped are generally of low enough energy to reach the end of the jet without significant energy loss, except if a relatively high level of optical emission must be explained as synchrotron radiation. The knotty nature could then be understood as variable output in the jet [e.g., 191]. However, in nearby FRII radio-galaxy jets, where synchrotron X-ray emission is seen (§3.4), the need for particle acceleration is secure, and similar underlying processes are expected in quasars even where the synchrotron X-rays might be outshone by beamed iC-CMB emission.

Details of the regions of particle acceleration are best studied in the closest sources. Cen A (Fig. 15) and NGC 315 (Fig. 1) are particularly good examples of FRI jets where the X-ray jet emission is resolved across as well as along the jet, and X-ray knots are embedded in more diffuse structure [97; 221; 100; 223]. The fact that the X-ray emission is not just confined to regions within energy-loss light travel distances of the knots shows that particle acceleration can occur also in diffuse regions. The relatively soft X-ray spectrum seen in the diffuse emission in Cen A has been used to argue that something other than shock acceleration (proposed for the knots) might be taking place in the diffuse regions [100], although no specific explanation is suggested, and the competition between energy losses and acceleration may be more important here.

5.2 Particle acceleration in knotty structures

The model of jet deceleration through entrainment (§4) leaves unanswered important questions about the origins of the bright knots that appear in many jets, particularly FRIs, and that are usually interpreted as the sites of strong shocks. Radio studies have searched for high-speed knot motions, with apparent speeds greater than the speed of light having been noted in M 87 [19]. A proper-motion study of the knots in Cen A over a 10-year baseline found that some knots, and even some more diffuse emission, travel at about $0.5c$, indicative of bulk motion

rather than pattern speed [97]. This motion, coupled with the jet-to-counter jet asymmetry, suggests considerable intrinsic differences in the two jets, to avoid the jets being at an implausibly small angle to the line of sight.

Other knots in Cen A appear to be stationary, which might suggest that they result from intruders in the flow, such as gas clouds or high-mass stars [e.g., 75; 97]. Some of these have emission profiles in the X-ray and radio that are unexpected from a simple toy model where the electrons are accelerated and then advect down the jet, losing energy from synchrotron radiation. Instead the bulk of the radio emission peaks downstream from the X-ray within these knots, leading to suggestions that both radio and X-ray-emitting electrons are accelerated in the standing shock of a stationary obstacle, and a wake downstream causes further acceleration of the low-energy, radio-emitting, electrons [97]. The resulting radio-X-ray offsets, averaged over several knots, could give the radio-X-ray offsets commonly seen in more distant jets [e.g., 96; 219; 63].

The knots of Cen A are not highly variable in observations to date [100], but dramatic variability on a timescale of months is seen in a knot in the jet of M 87, and the X-ray, optical and radio light curves are broadly consistent with shock acceleration, expansion, and energy losses, although the timeline is currently too short for strong conclusions to be drawn [105].

It is important to study the location of jet knots within the flow, to see if that can provide a clue as to their nature. A particularly interesting example is NGC 315 [221]. Here the diffuse emission contains a knotty structure in the radio and X-ray that appears to describe an oscillatory filament (Fig. 1). Although the structure could be the result of a chance superposition of non-axisymmetric knots, the level of coherence led to suggestions that the knots might be predominantly a surface feature residing in the shear layer between the fast spine and slower, outer, sheath plasma. If this interpretation is correct, we might expect the X-ray spectra of the knots to be similar across the transverse width of the jet. However, the distinct knotty emission is only about 10% of the total in X-rays and radio along the ~ 2.5 kpc of projected jet length over which it is detected, and with a source distance of ~ 70 Mpc the observations did not allow the spectra of the knot and diffuse emission to be separated.

At 3.7 Mpc, Centaurus A is a much closer example of an FRI radio galaxy whose knots and diffuse emission are seen over a similar projected linear distance to that of NGC 315. An X-ray spectral study of Cen A's knots found a spectral steepening with increasing lateral distance from the jet axis, disfavoring these knots all residing in a shear layer [223]. A flatter X-ray spectrum is seen more central to the flow, and an alternative explanation to acceleration in stationary shocks is that the knots here might be formed by stronger turbulent cascades with more efficient particle acceleration. Knot migration under the influence of the shear flow might then be expected, and proper-motion studies might then distinguish between this interpretation and stationary shocks from stellar or gaseous intruders entering the flow [223].

5.3 Incorporating polarization data

There are no current X-ray missions with polarization capabilities. However, the radio and optical bands probe electron populations responsible for the X-ray emis-

sion, albeit at different electron energies. If the emission is synchrotron, polarization data provide our best handle on the direction and relative degree of alignment of the magnetic field. Radio observations show that the fields are relatively well ordered, although there is much complexity. Broadly, the magnetic fields in FR II jets tend to be parallel to the jet axis, whereas in FRI jets they are either predominantly perpendicular, or perpendicular at the jet centre and parallel near the edges, with the mixed configurations pointing to perpendicular fields associated with shocks and parallel fields from shear or oblique shocks [32].

Optical polarization measurements of resolved jet structures have been made with *HST*. So far these have mostly concentrated on nearby FRI radio galaxies, where the optical features are brighter and the emission mechanism is synchrotron radiation [for an atlas of polarization images see 156]. Work is under way to explore optical polarization in the jets of FR II radio galaxies and quasars. As mentioned in §3.4, the optical emission should be essentially unpolarized if it is an extension of a beamed iC-CMB X-ray component, in contrast to being of synchrotron origin.

The first jet to be studied in detail in both its radio and optical polarized emission was M 87, where there is evidence for strong shock acceleration in compressed transverse magnetic fields at the base of bright emitting regions, although the polarization fraction becomes low at the flux maxima [155]. Significant differences between the polarization structures seen in the optical and radio suggest that the sites of acceleration are different for different electron energies, with the strongest shocks, that provide acceleration to the highest energies, appearing in the most central parts of the jet [155]. Detailed work on 3C 15 shows a jet that narrows from the radio to the optical to the X-ray, showing that acceleration to the highest energies occurs more centrally to the flow, and a mixture of strong shocks and stratified flows can account for the broad features seen in the optical and radio polarization [63].

A third source for which optical and radio polarization data have been important is 3C 346 (Fig. 16). Here X-ray emission is associated with a bright radio and optical knot where the jet bends by 70° in projection (the X-ray emission peaks somewhat upstream of the radio, as seen in other sources), leading to a suggestion that the bending and X-ray brightening are the result of a strong oblique shock located in the wake of a companion galaxy [219]. Polarization data has supported the model by revealing a compressed and amplified magnetic field in a direction consistent with that of the proposed shock, in both the radio and optical [64, and see Fig. 16].

6 What is jet plasma made of?

Jets are presumed to obtain much of their energy from the infall of matter into a supermassive black hole. It is then natural to suppose that electromagnetic radiation would carry much of the energy from the system on the smallest scales, since a plausible mechanism for the extraction of energy is the twisting of magnetic field linked to the accretion disk [e.g., 138]. Fast interactions with the plasma environment and efficient particle acceleration should load the field with matter. In the resulting magnetohydrodynamic flow much of the momentum would be carried

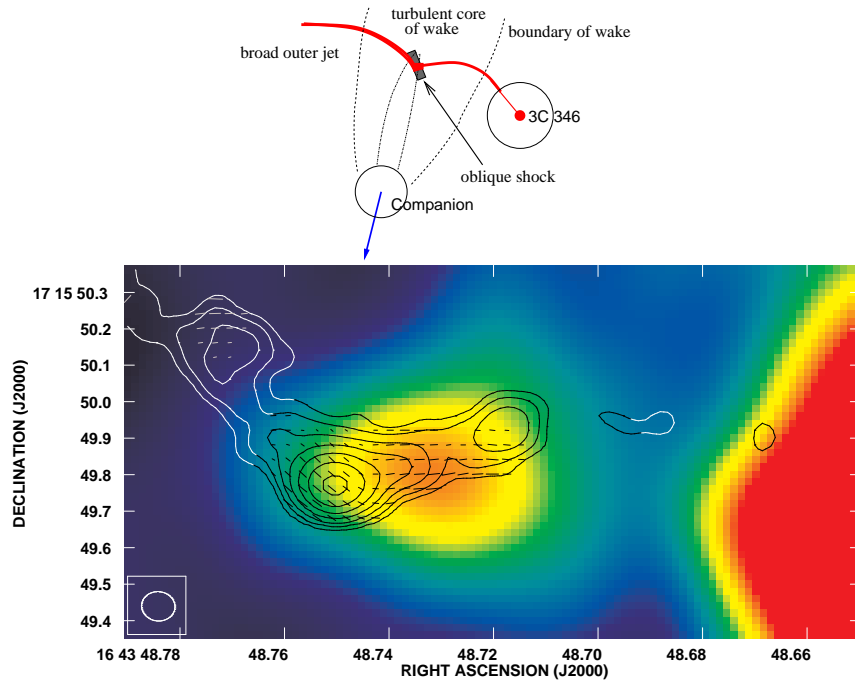


Fig. 16 3C 346. Upper: Schematic showing an oblique shock formed in the wake of the passage of a companion galaxy to 3C 346, and how it affects the radio jet, from [219]. Circles are the galaxies and red marks the path of the radio jet. Lower: Radio intensity contours and polarization vectors (rotated through 90° roughly to represent the magnetic-field direction) on a smoothed *Chandra* X-ray image, indicating compressed field lines aligned with the proposed shock, from [64].

by particles, although Poynting flux may carry a significant fraction of the total energy [163; 6].

Polarized radiation is the signpost to significant energy in relativistic particles and magnetic fields. Jet plasma must be neutral, on average, to remain collimated, but this can be achieved by various combinations of relativistic and cold electrons, positrons, and protons. Alternatively, it has been suggested that some of the energy is transported in a decaying neutral beam of ultra-high-energy neutrons and γ -rays [7].

Several quantities are available to help sort out the jet composition.

1. The synchrotron emission. Since the electron rest mass is only $1/1836$ that of a proton, and since synchrotron energy loss rates are proportional to the inverse square of mass, the observation of synchrotron radiation is usually used to infer the presence of relativistic electrons (and perhaps positrons), although an alternative model produces the synchrotron radiation from protons accelerated to energies greater than $\sim 10^{18}$ eV [2].
2. The jet power. All the particles, relativistic and thermal, combine with the magnetic field strength and bulk Lorentz factor to produce this quantity [see appendix B of 178]. It should be no smaller than the radiative power of the

old lobe material (the energy sink), averaged over the lifetime of the source. In cases where jets have excavated cavities in the external gas, the enthalpy can be estimated as that required to displace the gas [e.g., 23; 65; 4].

3. Faraday rotation. The contribution from thermal particles must not be so high as to exceed constraints placed by Faraday rotation, or by Faraday depolarization for extended regions.
4. The jet pressure. Relativistic particles and magnetic field are thought to dominate this quantity, which is $1/3$ of their energy density, and which can be compared to the external gas pressure. If X-ray inverse Compton emission is observed the internal energy density can be estimated using the radio synchrotron and X-ray flux densities (§2.2). Otherwise it is usual to assume minimum energy (§2.1). A difficulty is that relativistic electron-proton and electron-positron jets give similar pressures with different assumptions about the least energetic particles, for which observational constraints are poor at best. The contribution of thermal particles to the pressure is usually taken to be small.

Radiation drag and observational constraints on Comptonized radiation by cold electrons and positrons seriously hamper electron-positron jets formed close to the central black hole [185; 186]. In the cores of some quasars the radiated power is too large to be met by that contained in a jet of magnetic field and relativistic leptons close to minimum energy, and observational constraints on Comptonized radiation limit the density of cold leptons, so that a significant proton component is required if the energy carrier is indeed particles [196]. Thus, an electron-proton plasma is usually favoured when jets are discussed.

The presence of relativistic protons is supported for some FRI radio galaxies: the lobes, if assumed to be lepton-dominated and radiating at minimum energy (§2.2) would collapse under the pressure of the X-ray-emitting medium unless there is an additional pressure source and, although there are several ways of boosting the internal pressure in such a situation, magnetic dominance would make the sources unusual, electron dominance is unlikely from constraints on inverse-Compton scattering of the CMB, and non-relativistic protons are disfavoured on grounds of Faraday rotation, leaving a relativistic proton component most likely [e.g., 53]. However, decreased filling factors cannot be ruled out [e.g., 65], except perhaps where the radio structure has excavated a clear cavity in the X-ray-emitting atmosphere [e.g., 24]. If indeed the extra pressure is from relativistic protons, it is uncertain as to how much arises from entrained material accelerated in the shear layer of the decelerating jet as compared to particles transported from the core (see §4).

FRII jets transport more energy to larger distances, and thus have more need than FRI jets for a non-radiating energy carrier with high momentum transport. Relativistic hydrodynamic simulations find that the key parameter in preventing jets from strongly decelerating in an external boundary layer is density contrast with the external medium, in the sense that denser jets can propagate further [167]. A more dominant relativistic proton content could provide this. Protons are also required if the low-frequency spectral turn-over in hotspots is the result of cyclotron resonant absorption [e.g., 91]. On the other hand, pressure balance has been used to argue against relativistic protons in some FRII lobes. It is argued that the presence of relativistic protons is improbable since (a) the lobe magnetic field based on synchrotron and inverse Compton emission agrees with that from

minimum energy calculated using relativistic leptons alone, and (b) that, even in the absence of such protons, the source is in pressure balance with the external medium [e.g., 10; 54]. However, these calculations ignore possible dynamical effects in FRII lobes, and there are considerable additional sources of uncertainty (see §2.2 and item 4 above).

In the context of the beamed iC-CMB model for quasar jets (§3.2), it is possible to extend an argument limiting the density of cold electron-positron pairs [186] to kpc-scale regions [82]. In the case of PKS 0637-752, upper limits on Comptonized CMB radiation from *Spitzer* are sufficiently low to place stringent limits on the mass flux carried by cold lepton pairs, with the implication that this jet is indeed made electrically neutral through a strong presence of protons [203]. However, this argument relies on the beamed iC-CMB model being correct, with a large kinematic power being sustained throughout the jet (see §3.3).

Jet composition remains uncertain, and various degeneracies between physical quantities and observable parameters render it difficult to make watertight arguments. However, X-ray measurements continue to provide important clues to the puzzle.

7 What does X-ray emission tell us about the dynamics and energetics of radio plasma/gas interactions?

7.1 Expectations for FRIIs

The energy and momentum fluxes in FRII jets are expected to be sufficient to drive a bow shock at supersonic speed into the ambient medium [e.g., 134]. Ambient gas crossing the bow shock will be heated. For a shock advance speed relative to the speed of light of v_{adv}/c , the Mach number, \mathcal{M} , in monatomic gas of normal cosmic abundances with thermal energy kT in units of keV, is given by

$$\mathcal{M} \sim 580(v_{\text{adv}}/c)(kT)^{1/2}. \quad (15)$$

For a non-relativistic equation of state ($\gamma = 5/3$), the jump conditions for a non-radiating shock [e.g., 189] find that pressure, density, and temperature ratios between gas that has crossed the shock and the ambient medium are

$$P_2/P_1 = (5\mathcal{M}^2 - 1)/4 \quad (16)$$

$$\rho_2/\rho_1 = 4\mathcal{M}^2/(\mathcal{M}^2 + 3) \quad (17)$$

$$T_2/T_1 = (5\mathcal{M}^2 - 1)(\mathcal{M}^2 + 3)/16\mathcal{M}^2 \quad (18)$$

where subscripts 2 and 1 refer to post-shock and pre-shock conditions, respectively. For high advance speed and large Mach number the density contrast reaches a factor of four, resulting in enhanced X-ray emissivity from shocked gas. The visibility in observations will depend on the relative volumes of shocked and unshocked gas along given lines of sight.

Complications apply in reality. Firstly, there is observational evidence that in supernova remnants the post-shock electrons are cooler than the ions [e.g., 109;

160]. Secondly, a bow shock around a lobe is oblique away from its head, with a consequent change in the jump conditions and the emissivity contrast [210]. The closer a structure is to a spherical expansion, the more normal the shock will be everywhere and the better the applicability of the above equations.

ROSAT data revealed the presence of X-ray cavities coincident with the inner parts of the radio lobes of Cygnus A, and these were interpreted as due to the contrast between undisturbed ambient gas and gas around the lobes that had been heated in the past but has now expanded and cooled to a low emissivity [42], although the parameters of the shock are not effectively constrained by the data. More recent *Chandra* observations of Cygnus A find gas at the sides of the lobes to have $kT \sim 6$ keV, slightly hotter than the value of 5 keV from ambient medium at the same cluster radius, but the gas may have cooled after bow-shock heating, and again the data do not usefully constrain model parameters [188]. Evidence of strong shock heating around more distant FR II radio galaxies has yet to be seen.

CSS and GPS sources have been examined for evidence of shock heating. These are good places to look as the radio sources are generally considered to be in an early stage of expansion and they are overpressured with respect to even a cluster ambient medium [e.g., 184]. The disadvantage is that source sizes are small so that even *Chandra* will have difficulty in separating emission from the nuclei, radio structures, and ambient medium from that of any shocked gas. The best evidence for detection of shocked gas thus arises from deep XMM-Newton spectroscopy, and in particular that of the CSS source 3C 303.1 [152]. The X-ray spectrum contains soft emission (associated with the ambient galaxy atmosphere) and a hard component. Since nuclear emission is undetected in the radio, it is reasonable to associate the hard emission with shocked gas, and a model can be constructed [152] that has an expansion velocity consistent with cooling-time arguments for optical emission-line gas [61].

7.2 Dynamics of FRIs in clusters

Low-power sources are closer and more amenable to detailed study, since the various components of X-ray emission are more easily separated. The medium plays an important rôle in the deceleration of the jets, which share momentum and energy with entrained material (§4).

The *Einstein* and *ROSAT* missions found evidence that the radio lobes of NGC 1275 have pushed Perseus-cluster gas aside [e.g., 28], and now many clusters and groups are found to harbour gas cavities containing radio plasma that originates from active galaxies [e.g., 23]. Rather than expansion at high Mach number, the displacement of the gas appears normally to create low-density, rising bubbles in rough pressure balance with the surrounding medium [e.g., 50]. NGC 1275, M 87, and Hydra A are showcase examples with deep *Chandra* exposures and complex bubble and cavity systems [72; 78; 213]. Radio bubbles in clusters are sufficiently common that they are an important heat source today, with enough power to balance the radiative cooling of dense gas in clusters [e.g., 65; 159], although the total energies and lifetimes of individual bubbles are considerably uncertain. An issue of particular interest that follows from this is the potential for the associated heating and cooling to forge the link between black-hole and galaxy

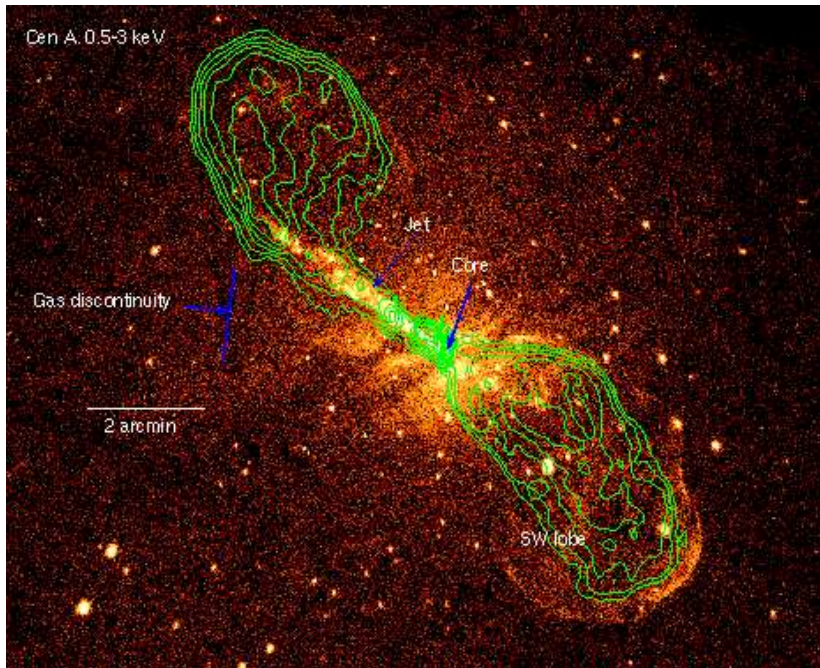


Fig. 17 Radio contours on a deep *Chandra* image of Cen A, showing the core and NE jet crossed by absorption stripes corresponding to NGC 5128's dust lanes, the SW lobe, structures associated with the NE lobe, the position of a merger-related gas discontinuity that shows up better at lower energies, and many XRBs in NGC 5128 [see 100; 114; 223; 127; 187].

growth. A recent review is available [144], and so the topic is not dealt in depth here.

It is noteworthy that the luminosity function of radio sources places the energetically dominant population to be roughly at the FRI/FRII boundary [e.g., 136], rather than within the more numerous but lower power population of FRIs studied in nearby clusters (although there are claims that total jet power scales slightly less than linearly with radio power [e.g., 211; 24]). It thus remains possible that the rather gentle heating around currently studied sources does not provide us with the complete picture, and violent shock heating around more powerful sources is energetically important but currently eluding detection.

7.3 Centaurus A

The best example of supersonic expansion is not in an FRII radio source but associated with the inner southwest radio lobe of Cen A [124, and see Fig. 17 for a more recent, deeper, *Chandra* image]. Cen A is our nearest radio galaxy, where 1 arcmin corresponds to ~ 1.1 kpc. The full extent of Cen A's radio emission covers several degrees on the sky [117]. Within this lies a sub-galaxy-sized double-lobed inner structure [36] with a predominantly one-sided jet to the NE and weak counter-jet knots to the SW [97] that are embedded in a radio lobe with pressure

at least ten times larger than that of the ambient ISM [124]. The lobe should be expanding and be surrounded by a shock. The associated structure is exquisitely seen in Figure 17. Although the capped SW lobe is around the weak counterjet, so it is not evident that the lobe is being thrust forward supersonically with respect to the external interstellar medium (ISM) by the momentum flux of an active jet, the high internal pressure in the radio lobe ensures its strong expansion.

The density contrast between post-shock and pre-shock gas in Cen A inferred by [124] was larger than four, which is not allowed by Equation 17, and so straightforward modelling was not possible. New modelling is underway using results from the new deep observation. However, the conclusion that the lobe's kinetic energy exceeds its thermal energy, and the thermal energy of the ISM within 15 kpc of the centre of the galaxy, is unlikely to change. As the shell dissipates, most of the kinetic energy should ultimately be converted into heat and this will have a major effect on Cen A's ISM, providing distributed heating.

There is much still to be learned about how gas is displaced by radio structures, and the processes of heat transfer. A new view will be possible with the high-resolution spectroscopic capabilities of the International X-ray Observatory currently under study by ESA and NASA. This will provide the vital ingredient of useful velocity data, giving a handle also on such issues as turbulence and non-perpendicular velocities at shocks.

7.4 The effect of galaxy mergers

It is important to understand what triggers radio activity and what causes it to cease, particularly since radio sources are now recognized as an important heat source for large-scale structure (§ 7.2). It has long been recognized that mergers may be important in *triggering* radio activity, and this is consistent with the preference for low-power radio galaxies to reside in clusters and rich groups. For example, NGC 1275 and M 87 (§ 7.2) are the dominant galaxies of the Perseus and Virgo clusters, respectively. Cen A (§ 7.3) is hosted by NGC 5128 which in turn hosts an inner warped disk suspected to be the merger remnant of a small gas-rich spiral galaxy [e.g., 158].

Mergers leave an imprint on the temperature, density, and metallicity structures of the gas. Due to good linear resolution it is again Cen A that shows such effects particularly well, with clear indications that even the hot X-ray-emitting gas is poorly mixed. The merger appears to be having an important influence on the evolution of the northeast radio jet and inner lobe [127].

In the more extreme case of 3C 442A (Figure 18) there is evidence that a merger may have smothered a previously active jet, leaving a large volume of decaying radio plasma, while at the same time re-starting jet activity in the nucleus of one of the galaxies [222]. Here the merger gas has sufficiently high pressure for the radio lobes to be riding on the pressure front of the merger gas that is sweeping them apart. The energy in the merger gas will eventually be dissipated in the outer regions of the group atmosphere — an additional source of heating to that arising from both the old and new merger-induced radio activity. The radio spectrum from the old decaying radio lobes is flatter where they are being compressed by the expanding merger gas, suggesting that energy from the gas has a second effect, in re-exciting relativistic electrons through compression and adiabatic heating [222].

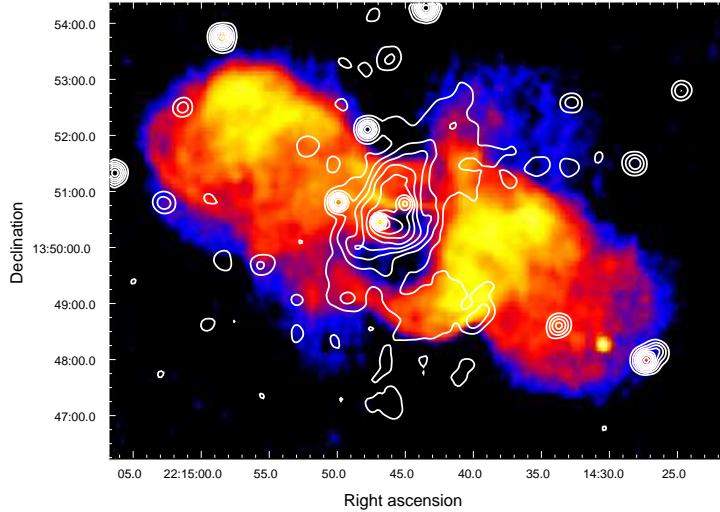


Fig. 18 *Chandra* contours (logarithmic spacing) on a color radio image of 3C 442A, taken from [222]. Bright X-ray emission from the merger atmospheres of NGC 7236 and NGC 7237 fills the gap between the radio lobes which are no longer fuelled by an active jet.

While it is undoubtedly true that mergers produce messy substructures, the example of 3C 442A suggests that there is some prospect that the switching on and off of radio activity by mergers can be timed (albeit roughly) using the morphology of the stellar component of the galaxies and spectral changes in the radio plasma, and that this can be combined with the measured energy content of the gas and radio plasma to trace the history of radio outbursts and their effectiveness in heating gas.

8 Is a jet's fate determined by the central engine?

8.1 An evolutionary cycle?

The Ledlow-Owen relation (§1.3) showed that a galaxy of a given optical luminosity can host either an FRI or FR II radio source. This resulted in renewed speculation in the 1990s that there may be an evolution between FR II and FRI activity controlled by external influences. Such speculation was supported by evidence of FR IIs associated with galaxy mergers (distorted isophotes and higher amounts of high-excitation ionized gas) and FR Is associated with galaxies in more relaxed dynamical states [17]. Evolutionary ideas have also arisen from the so called 'fundamental plane' that places AGN on an extension of the relationship between inner jet radio power, X-ray luminosity and black-hole mass found for X-ray binaries (XRBs) [146; 73]. It has been suggested that the changes in X-ray spectrum and jet luminosity that accompany changes in accretion characteristics in an XRB could apply to AGN, such that an individual object may go through transitions between an FRI and FR II, and indeed to becoming radio quiet [e.g., 123].

Observationally, kpc-scale jets accompany AGN with accretion flows that in the extreme are either geometrically-thick and radiatively inefficient or geometrically-thin and radiatively efficient, with the latter accompanied by high-excitation optical emission lines. It is possible that an AGN changes over the lifetime of a radio source, such that the observed kpc-scale radio structures are the result of ejection from an AGN evolving through different states. Some sort of intermittency of the central engine over timescales of $\sim 10^4 - 10^6$ years (shorter than the lifetime of radio sources, §1.4) gains support from observational and theoretical considerations [e.g., 164; 176; 111; 191]. Multiple changes to the central structure over the lifetime of the radio source would be required to reconcile the claim that a geometrically-thick flow is needed to sustain a significant jet (with the most powerful requiring a spinning black hole) [145] with the observation that many AGN with powerful jets currently show geometrically-thin disks and high-excitation emission lines (see below).

Closer examination is needed of the extent to which the observed powers and structures of jets relate either to the accretion processes or to large-scale environmental effects. Both appear to play a rôle.

8.2 The rôle played by accretion processes

Broadly, powerful jets of FR II structure are associated with AGN showing high-excitation optical emission lines, while lower-power jets, normally but not always of FR I structure, are associated with AGN showing low-excitation lines. This suggests that the central engine has at least some influence on the power and large-scale structure of the jets [e.g., 9].

A correlation between the core radio emission and low-energy (~ 1 to 2 keV) nuclear X-ray output of radio galaxies has been known since the *Einstein* and *ROSAT* missions, and has been used to argue that the soft X-rays arise from pc-scale jets [70; 214; 37; 93]. An optical core is often seen with *HST*, and is interpreted as synchrotron emission from a similar small-scale emitting region [47; 94; 40; 49; 207]. Such pc-scale jets protrude from any gas and dust torus invoked by AGN unified models, and so this component should not be greatly affected by absorption, although relativistic effects will cause jet orientation to affect the level of X-ray flux observed.

Since jet emission dominates at low X-ray energies, it has been important to obtain sensitive spectral measurements that extend to the higher X-ray energies accessible to *Chandra* and *XMM-Newton* in order to probe the region closer to the SMBH and representative of the bolometric power of the central engine. At these energies any strong emission from the AGN should dominate jet emission even if it is largely absorbed at lower energies by a gas torus. Results find a number of radio galaxies showing clear evidence of a hard continuum, sometimes accompanied by Fe-line emission, and presumed to be emission associated with an accretion-disk corona [e.g., 204; 224; 90]. Both the jet and central-engine X-ray components can sometimes be distinguished in the same spectrum [e.g., 54; 67; 225].

The hard component is more often detected in FR IIs than in FR Is. Of course, greater absorption from a torus could potentially combine with lower X-ray luminosity in causing the non-detection of the second component in most FR Is, and so particular reliability can be placed on the results of a study of nearby ($z < 0.1$)

radio galaxies that has allowed for absorption in placing upper limits on the luminosity of undetected nuclear components [69]. The radiative efficiency of the central engine was then found by correcting the X-ray luminosity to a bolometric luminosity and combining it with the inferred SMBH mass. In powerful FRIIs, radiatively-efficient accretion associated with a thin disk surrounded by an obscuring torus is normally inferred. FRII radio galaxies at $z \sim 0.5$ also show an absorbed X-ray component [11]. In contrast, in $z < 0.1$ FRIIs, all the nuclear X-ray emission can normally be interpreted as jet related, and usually only upper limits are found for accretion-related emission [69]. Any X-ray luminosity associated with a non-jet central-engine component in low-power sources is normally sufficiently low to support earlier speculations based on the Ledlow-Owen relation that the physical difference between the two types of radio source arises from the different nature of their accretion disks and efficiency of accretion [85]. Further support for these ideas comes from *Spitzer* results for the $z < 0.1$ sample [22] that show an additional component of hot dust only in FRIIs.

While results at first-look appear quite convincing of a connection between large-scale radio power and the structure of the central engine, there are sources which defy the trend. Both Cen A and NGC 4261 have large-scale FRI structures, and yet contain absorbed, hard, luminous X-ray components characteristic of the coronae of thin accretion disks seen through an obscuring torus [67; 225]. This might suggest that something relatively recent (perhaps the galaxy merger in the case of Cen A [69]) has provided additional material for accretion and affected the central engine in a way that has yet to be reflected in the power and structure of the large-scale radio emission. The difficulty is that merger and source-development time scales are expected to be comparable. A further complication is the tendency for any X-ray accretion-related components in FRII low-excitation radio galaxies to be less luminous than those seen in a typical FRII high-excitation radio galaxy [99], as was known for the optical continuum [49; 206]. This means that not all FRIIs have equivalent central engines. However, it is hard to treat as a coincidence the tendency for the most powerful FRIIs with the least evidence for external disruption to arise from AGN showing high-excitation optical emission lines and evidence for thin accretion disks.

In the normally inferred absence of thin radiatively-efficient accretion disks in FRIIs, it has been argued in several cases that sufficient X-ray-emitting hot gas is present in their galaxies and clusters to produce the required jet power through a geometrically-thick Bondi accretion flow [e.g., 62; 4]. Here the jet power is inferred from the energy required to excavate the cavities observed in the X-ray-emitting gas, i.e., a more direct method than scaling from radio power [e.g., 211] as is normal in the absence of other information. Recent work confirms that the most luminous FRIIs also tend to lie in luminous X-ray clusters [12], and it is reasonable to assume that they experience similar or greater supplies of galaxy and cluster hot gas. However jet powers are also higher (how much so rests on uncertainties in speed and composition), consistent with requiring an extra energy source in the form of stars and gas clouds fuelling a thin accretion disk. A major outstanding problem is a full understanding of the mechanisms which convert gas infall into two different accretion structures. Jets are expected to be more strongly coupled to the structure of the host stellar system, and hence to play a more major rôle in feedback, if the accreting gas originates predominantly from the reservoir

contained in the potential well of the system as a whole, whether it be hot [e.g., 4] or cold [e.g., 161] in origin.

8.3 The rôle of the environment

Assuming that jets are genuinely symmetric at production, the environment appears to be, at a minimum, a strong secondary factor (with jet power being the likely primary influence) in shaping large-scale jet structure. For example, some radio sources show what appears to be FRI morphology on one side and FR II on the other, and this has been used to argue for different environmental effects on the two sides [92].

VLBI proper-motion studies find few, if any, differences in the speed or morphology of FRI and FR II radio jets in their initial stages of development from the central engine [154; 88]. However, the radiative powers are higher in FR IIs, but not in linear proportion to their total radio powers [e.g., 87; 89], suggesting that on the small scale a radio source has knowledge of how it will evolve. Particularly compelling evidence that the environment does have some influence is the recent discovery that quasars, traditionally the hosts only of FR II structures, can host FRI radio structures, with evidence that denser, more clumpy, environments at higher redshift are allowing this to occur [107]. The rôle of the X-ray-emitting environment in decelerating FRI jets was discussed in §4.

8.4 Information from beamed sources

The beamed counterparts of radio galaxies (quasars and BL Lac objects) do not allow the accretion structures to be probed in the X-ray, since the beamed jet emission swamps all other nuclear components; indeed it is sometimes dominant up to the TeV band. Multi-wavelength spectral energy distributions and variability time scales are used to probe the beaming parameters and the physical properties of the emitting regions [e.g., 84; 128; 193]. Correlated flares are sometimes measured across wavebands, giving support to the presence of a dominant spatial region of emission [e.g., 205; 194], but otherwise uncertainties of size scales, geometries, and parameters for the competing processes of energy loss and acceleration often force the adoption of oversimplified or poorly-constrained models for individual jets. Much is published on the topic, and a review is beyond the scope of this work. Substantial progress in understanding is anticipated from multiwavelength programmes associated with the Fermi Gamma-ray Space Telescope.

VLBI radio-polarization studies have found systematic differences between powerful quasars (beamed FR IIs) and BL Lac objects (beamed FR Is) in core polarizations, the orientations of the magnetic fields in the inner jets, and in jet length, although it is difficult to separate intrinsic differences from the possible influence of the parsec-scale environment, such as the density and magnetic field contained in line-emitting gas [43].

9 Summary and concluding remarks

The last decade has seen massive progress in our understanding of the X-ray properties of extragalactic radio jets and their environments. *Chandra*'s sub-arcsec spatial resolution has been of paramount importance in measuring resolved X-ray emission from kpc-scale jet structures, and in extending studies of X-ray nuclei to sources other than beamed quasars and BL Lac objects by separating the emission of weaker nuclei from that of the jets and X-ray emitting environments.

The assumption that radio structures roughly lie in a state of minimum energy between their relativistic particles and magnetic fields is broadly verified in a few tens of sources through combining X-ray inverse Compton with radio synchrotron data (§2.2). This is the assumption commonly adopted in the absence of other information, and so its verification is reassuring, although much sub-structure is likely to occur and there is no reason to expect minimum energy to hold in dynamical structures.

The increase in numbers of known resolved kpc-scale X-ray jets has been remarkable, from a handful to the several tens of sources that *Chandra* has mapped in detail. There are grounds to believe that there are X-rays from synchrotron radiation in sources both of FRI and FRII types (§5.1), requiring in-situ particle acceleration to TeV energies. The steepening in spectral slope which most commonly occurs at infra-red energies may be related more to acceleration processes than energy losses, but more multiwavelength observational work is required to characterize the acceleration sites and support a theoretical understanding. The fact that X-ray synchrotron emission with an X-ray to radio flux-density ratio, $S_{1 \text{ keV}}/S_{5 \text{ GHz}}$, between about 10^{-8} and 10^{-7} is so common in jets where the bulk flow is inferred to be relativistic implies that there will be many more X-ray jet detections with current instrumentation in sufficient exposure time.

The dominant X-ray emission mechanism in resolved quasar jets remains uncertain, but it is likely that beamed emission from scattering of CMB photons is dominant in jets at small angles to the line of sight. This requires that highly relativistic bulk flows exist far from the cores, contradicting earlier radio studies but possibly understandable in the context of transverse velocity profiles. The knotty appearance of these jets is then possibly a result of variable output from the nuclei. Much of the knotty X-ray appearance of FRI jets, on the other hand, likely arises from spatial variations in the strength of particle acceleration (§5.2).

Jet theory has had some pleasing successes, such as the agreement between X-ray pressure profiles and predictions from hydrodynamical models for low-power jets in the regions where they are believed to be slowed by entrainment of the external medium or stellar mass loss (§4).

We are still largely ignorant of jet composition, and this is a difficult problem to solve since jet dynamics are governed by the energy of the constituent particles rather than their mass. There is generally growing support for a strong presence of relativistic protons (§6).

The observation of bubbles and cavities in cluster gas produced dynamically by radio structures has renewed interest in the mechanisms by which active galaxies introduce heat into gaseous atmospheres. A few nearby bright systems have been the subject of intense study with *Chandra* (§7.2). Although the way in which energy is deposited on the large scale is still far from clear, information on mor-

phology and temperature has been used to infer the underlying energetics of the structures.

An area where work is still in its infancy is that of understanding the triggering of radio sources, and the possible rôle played here by galaxy and cluster mergers in promoting or inhibiting radio-source development (§7.4). The emerging picture shows that very different accretion structures can host radio jets, with a tendency for quasar-type nuclei to be associated with more powerful jets. How jets are powered by these different accretion structures and gas infall, and the duration of a given mode relative to typical lifetimes of radio sources, remain to be better understood.

The future is bright. *Chandra* and *XMM-Newton* are now mature observatories. Operational experience is enabling both more ambitious and more speculative programs to be undertaken. For example, *Chandra* is completing sensitive exposures of all 3CRR radio sources within a redshift of 0.1, and a large shallow survey of quasar jets to study the X-ray-emission mechanism in a statistical sense and seek out more sources for deep, detailed study. Observations of a somewhat more speculative nature are also being made, such as observing radio sources of different inferred ages, and studying how galaxy and cluster mergers are impacting the radio-source structures and their influence on the surrounding atmospheres. These are just examples. At the same time, *Suzaku* is making spectral measurements of active-galaxy nuclei, and testing the spin characteristics of black holes hosting radio sources through searching for relativistic broadening in Fe lines. We can expect fantastic results from continuing X-ray work, and many surprises.

New facilities coming on line will enrich the X-ray results. *Spitzer* has measured dust, stars, and non-thermal cores in the centres of radio galaxies, placing constraints on the central structures. It has also detected a number of kpc-scale jets, helping to tie down the all-important breaks in the spectral distributions of the synchrotron radiation that are likely to be connected to the process of particle acceleration. *Herschel* will continue such work.

The characteristics of the non-thermal emission at energies higher than the X-ray provide a sensitive test of emission mechanisms and a probe of jet composition. The Fermi Gamma-ray Space Telescope is providing such data, particularly for the embedded small-scale jets of highly-beamed quasars and BL Lac objects, as are ground-based Cerenkov telescopes sensitive to TeV emission.

ALMA will probe the cool component of gas in active galaxies, and provide information on one possible component of accretion power. Radio measurements with *e-MERLIN* and *EVLA* will probe spatial scales intermediate between pc and kpc, important in the launching and collimation of jets. They will also provide improved information on transverse jet structure.

Extending polarimetry to the X-ray, as is under study in the community, will provide key tests of jet emission and acceleration mechanisms, just as such work with *HST* is starting to do in the optical. Most importantly, a future X-ray observatory that has the sensitivity and spectral resolution to probe gas dynamics associated with radio sources is crucial for confirming and extending source modelling that is currently in its infancy. Such capabilities will come with the launch of a new facility such as the International X-ray Observatory currently under study by ESA and NASA.

Acknowledgements I am grateful to Mark Birkinshaw for his essential contributions to our collaborative work on radio sources since the early 1990s, when we first observed radio galaxies with *ROSAT*. More recently, colleagues and students too numerous to list have energetically worked on jet data, and helped feed my enthusiasm for the subject. I particularly thank all involved in making *Chandra* such a great success, permitting resolved X-ray emission to be seen so clearly in so many active-galaxy jets. The outline for this review has evolved from talks I gave at ‘6 Years with *Chandra*’, Cambridge MA, November 2005, and ‘Observations from High Energy Astrophysics Satellites’ at the Marcel Grossmann meeting, Berlin, July 2006, and I am grateful to the organizers of those meetings for their invitations. I thank Raffaella Morganti, Thierry Courvoisier and Mark Birkinshaw for suggestions that have improved the manuscript. The NASA Astrophysics Data System has greatly assisted me in constructing the bibliography for this review.

References

1. Achterberg A, Gallant YA, Kirk JG, Guthmann AW (2001) Particle acceleration by ultra-relativistic shocks: theory and simulations. *MNRAS* 328: 393–408
2. Aharonian FA (2002) Proton-synchrotron radiation of large-scale jets in active galactic nuclei. *MNRAS* 322: 215–230
3. Alexander P, Leahy JP (1987) Ageing and speeds in a representative sample of 21 classical double radio sources. *MNRAS* 225: 1–26
4. Allen SW, Dunn RJH, Fabian AC, Taylor GB, Reynolds CS (2006) The relation between accretion rate and jet power in X-ray luminous elliptical galaxies. *MNRAS* 372: 21–30
5. Amato E, Arons J (2006) Heating and nonthermal particle acceleration in relativistic, transverse magnetosonic shock waves in proton-electron-positron plasmas. *ApJ* 653: 325–338
6. Appl S, Camenzind M (1993) The structure of relativistic MHD jets: a solution to the nonlinear Grad-Shafranov equation. *A&A* 274: 699–706
7. Atayan A, Dermer CD (2004) Synchrotron versus Compton interpretations for extended X-ray jets. *ApJ* 613: 151–158
8. Barthel PD (1989) Is every quasar beamed? *ApJ* 336: 606–611
9. Baum SA, Zirbel EL, O’Dea CP (1995) Toward understanding the Fanaroff-Riley dichotomy in radio source morphology and power. *ApJ* 451: 88–99
10. Belsole E, Worrall DM, Hardcastle MJ, Birkinshaw M, Lawrence CR (2004) *XMM-Newton* observations of three high-redshift radio galaxies. *MNRAS* 352: 924–938
11. Belsole E, Worrall DM, Hardcastle MJ (2006) High redshift FR II radio galaxies: X-ray properties of the cores. *MNRAS* 366: 339–352
12. Belsole E, Worrall DM, Hardcastle MJ, Croston JH (2007) High redshift Fanaroff-Riley type II radio sources: large scale X-ray environment. *MNRAS* 381: 1109–1126
13. Berghöfer TW, Bowyer S, Korpela E (2000). Extreme Ultraviolet Explorer observations of clusters of galaxies: Virgo and M 87. *ApJ* 535: 615–620
14. Bicknell GV (1984) A model for the surface brightness of a turbulent low Mach number jet. I - Theoretical development and application to 3C 31. *ApJ* 286: 68–87
15. Bicknell GV (1986) A model for the surface brightness of a turbulent low Mach number jet. III - Adiabatic jets of arbitrary density ratio: Application to NGC 315. *ApJ* 305: 109–130
16. Bicknell GV (1994) On the relationship between BL Lacertae objects and Fanaroff-Riley I radio galaxies. *ApJ* 422: 542–561
17. Bicknell GV (1994) Extragalactic radio sources and the role of relativistic jets. *Aust. J. Phys.* 47: 669–680
18. Bird J, Martini P, Kaiser C (2008) The lifetime of FR II sources in groups and clusters: implications for radio-mode feedback. *ApJ* 676: 147–162
19. Biretta JA, Zhou F, Owen FN (1995) Detection of proper motions in the M87 jet. *ApJ* 447: 582–596
20. Birkinshaw M (1991) The stability of jets. In: Hughes PA (ed) *Beams and Jets in Astrophysics*. Cambridge University Press, pp. 278–341
21. Birkinshaw M, Worrall DM, Hardcastle MJ (2002) The X-ray jet and halo of PKS 0521-365. *MNRAS* 335: 142–150

22. Birkinshaw M, et al. (2006) IR and X-ray cores in low-redshift active galaxies. *BAAS*, 38, 353, and (2008), work in preparation
23. Birzan L, Rafferty DA, McNamara BR, Wise MW, Nulsen PEJ (2004) A systematic study of radio-induced X-ray cavities in clusters, groups, and galaxies. *ApJ* 607: 800–809
24. Birzan L, McNamara BR, Nulsen PEJ, Carilli CL, Wise MW (2008) Radiative efficiency and content of extragalactic radio sources: toward a universal scaling relation between jet power and radio power. *ApJ* 686: 859–880
25. Blandford RD, Eichler D (1987) Particle acceleration at astrophysical shocks — a theory of cosmic-ray origin. *Physics Reports* 154: 1–75
26. Blumenthal GR, Gould RJ (1970) Bremsstrahlung, synchrotron radiation, and Compton scattering of high-energy electrons traversing dilute gases. *Rev. Mod. Phys* 42: 237–271
27. Blundell KM, Fabian AC, Crawford CS, Erlund MC, Celotti A (2006) Discovery of the low-energy cutoff in a powerful giant radio galaxy. *ApJ* 644: L13–L16
28. Böhringer H, Voges W, Fabian AC, Edge AC, Neumann DM (1993) A *ROSAT* HRI study of the interaction of the X-ray-emitting gas and radio lobes of NGC 1275. *MNRAS* 264: L25–L28
29. Böhringer H, et al. (2001) *XMM-Newton* observations of M 87 and its X-ray halo. *A&A* 365: L181–L187
30. Bondi M, Brunetti G, Comastri A, Setti G (2004) Anisotropic inverse Compton emission in the radio galaxy 3C 265. *MNRAS* 354: L43–L47
31. Bridle AH, Hough DH, Lonsdale CJ, Burns JA, Laing RA (1994) Deep VLA imaging of twelve extended 3CR quasars. *AJ* 108: 766–820
32. Bridle A, Perley RA (1984) Extragalactic radio jets. *ARAA* 22: 319–358
33. Brunetti G, Bondi M, Comastri A, Setti G (2002) *Chandra* discovery of extended non-thermal emission in 3C 207 and the spectrum of the relativistic electrons. *A&A* 381: 795–809
34. Brunetti G, Mack K-H, Prieto MA, Varano S (2003) In-situ particle acceleration in extragalactic radio hot spots: observations meet expectations. *MNRAS* 345: L40–L44
35. Burbidge GR (1956) On Synchrotron Radiation from Messier 87. *ApJ* 124: 416–429
36. Burns JO, Feigelson ED, Schreier EJ (1983) The inner radio structure of Centaurus A — Clues to the origin of the jet X-ray emission. *ApJ* 273: 128–153
37. Canosa CM, Worrall DM, Hardcastle MJ, Birkinshaw M (1999) X-ray Observations of low-power radio galaxies from the B2 catalogue. *MNRAS* 310: 30–38
38. Canvin JR, Laing RA (2004) Relativistic models of two low-luminosity radio jets: B2 0326+39 and B2 1553+24. *MNRAS* 350: 1342–1365
39. Canvin JR, Laing RA, Bridle AH, Cotton WD (2005) A relativistic model of the radio jets in NGC 315. *MNRAS* 363: 1223–1240
40. Capetti A, Celotti A, Chiaberge M, de Ruiter HR, Fanti R, Morganti R, Parma P (2002) The HST survey of the B2 sample of radio-galaxies: Optical nuclei and the FR I/BL Lac unified scheme. *A&A* 383: 104–111
41. Carilli CL, Perley RA, Dreher JW, Leahy JP (1991) Multifrequency radio observations of Cygnus A - spectral aging in powerful radio galaxies. *ApJ* 383: 554–573
42. Carilli CL, Perley RA, Harris DE (1994) Observations of interaction between cluster gas and the radio lobes of Cygnus-A. *MNRAS* 270: 173–177
43. Cawthorne TV, Wardle, JFC, Roberts, DH, Gabuzda DC (1993) Milliarcsecond polarization structure of 24 objects from the Pearson-Readhead sample of bright extragalactic radio sources. II. Discussion. *ApJ* 416: 519–535
44. Celotti A, Ghisellini G, Chiaberge M (2001) Large-scale jets in active galactic nuclei: multiwavelength mapping. *MNRAS* 321: L1–L5
45. Chartas G, et al. (2000) The *Chandra* X-ray observatory resolves the X-Ray morphology and spectra of a jet in PKS 0637-752. *ApJ* 542: 655–666.
46. Chiaberge M, Gilli R, Macchetto FD, Sparks WB, Capetti A (2003) What do the Hubble Space Telescope and *Chandra* tell us about the jet and the nuclear region of the radio galaxy 3C 270? *ApJ* 582: 645–653
47. Chiaberge M, Capetti A, Celotti A (1999) The HST view of FR I radio galaxies: evidence for non-thermal nuclear sources. *A&A* 349: 77–87
48. Chiaberge M, Celotti A, Capetti A, Ghisellini G (2000) Does the unification of BL Lac and FR I radio galaxies require jet velocity structures? *A&A* 358: 104–112

49. Chiaberge M, Capetti A, Celotti A (2002) Understanding the nature of FR II optical nuclei: a new diagnostic plane for radio galaxies. *A&A* 394: 791–800
50. Churazov E, Brügggen M, Kaiser CR, Böhringer H, Forman W (2001) Evolution of buoyant bubbles in M 87. *ApJ* 554: 261–273
51. Comastri A, Brunetti G, Dallacasa D, Bondi M, Pedani M, Setti G (2003) Inverse Compton X-rays from the radio galaxy 3C 219. *MNRAS* 340: L52–L56
52. Conway JE (2002) Compact symmetric objects — newborn radio galaxies? *New Astronomy Reviews* 46: 263–271
53. Croston JH, Hardcastle MJ, Birkinshaw M, Worrall DM (2003) *XMM-Newton* observations of the hot-gas atmospheres of 3C 66B and 3C 449. *MNRAS* 346: 1041–1054
54. Croston JH, Birkinshaw M, Hardcastle MJ, Worrall DM (2004) X-ray emission from the nuclei, lobes and hot-gas environments of two FR-II radio galaxies. *MNRAS* 353: 879–889
55. Croston JH, Hardcastle MJ, Harris DE, Belsole E, Birkinshaw M, Worrall DM (2005) An X-Ray study of magnetic field strengths and particle content in the lobes of FR II radio sources. *ApJ* 626: 733–747
56. Croston JH, Hardcastle MJ, Birkinshaw M, Worrall DM, Laing RA (2008) An *XMM-Newton* study of the environments, particle content and impact of low-power radio galaxies. *MNRAS* 386: 1709–1728
57. Croton DJ, et al. (2006) The many lives of active galactic nuclei: cooling flows, black holes and the luminosities and colours of galaxies. *MNRAS* 365: 11–28
58. Dermer CD (1995) On the beaming statistics of gamma-ray sources. *ApJ* 446: L63–L66
59. Dermer CD, Sturmer, SJ, Schlickeiser, R (1997) Nonthermal Compton and synchrotron processes in the jets of active galactic nuclei. *ApJ* 446: L63–L66
60. Dermer CD, Atayan AM (2002) X-ray synchrotron spectral hardenings from Compton and synchrotron losses in extended *Chandra* jets. *ApJ* 568: L81–L84
61. de Vries WH, O’Dea CP, Baum SA, Barthel PD (1999) Optical-radio alignment in compact steep-spectrum radio sources. *ApJ* 526: 27–39
62. Di Matteo T, Allen SW, Fabian AC, Wilson As, Young AJ (2003) Accretion onto the supermassive black hole in M87. *ApJ* 582: 133–140
63. Dulwich F, Worrall DM, Birkinshaw M, Padgett CA, Perlman ES (2007) The structure of the jet in 3C 15 from multi-band polarimetry. *MNRAS* 374: 1216–1226
64. Dulwich F, Worrall DM, Birkinshaw M, Padgett CA, Perlman ES (2008) Multi-band polarimetry of the oblique shock in the jet of the powerful radio galaxy 3C 346. *MNRAS*: submitted
65. Dunn RJH, Fabian AC, Taylor GB (2005) Radio bubbles in clusters of galaxies. *MNRAS* 364: 1343–1353
66. Eilek JA, Hughes PA (1991) Particle acceleration and magnetic field evolution. In: Hughes PA (ed) *Beams and Jets in Astrophysics*. Cambridge University Press, pp. 428–483
67. Evans DA, Kraft RP, Worrall DM, Hardcastle MJ, Jones C, Forman WR, Murray SS (2004) *Chandra* and *XMM-Newton* observations of the nucleus of Centaurus A. *ApJ* 612: 786–796
68. Evans DA, Hardcastle MJ, Croston JH, Worrall DM, Birkinshaw M (2005) *Chandra* and *XMM-Newton* observations of NGC 6251. *MNRAS* 359: 363–382
69. Evans DA, Worrall DM, Hardcastle MJ, Kraft RP, Birkinshaw M (2006) *Chandra* and *XMM-Newton* observations of a sample of low-redshift FR I and FR II radio galaxy nuclei. *ApJ* 642: 96–112
70. Fabbiano G, Miller L, Trinchieri G, Longair M, Elvis M (1984) An X-ray survey of a complete sample of 3CR radio galaxies. *MNRAS* 277: 115–131
71. Fabian AC, Celotti A, Johnstone RM (2003) *Chandra* reveals X-rays along the radio axis in the quasar 3C 9 at $z=2.012$. *MNRAS* 338: L7–L11
72. Fabian AC, Sanders JS, Taylor GB, Allen SW, Crawford CS, Johnstone RM, Iwasawa K (2006) A very deep *Chandra* observation of the Perseus cluster: shocks, ripples and conduction. *MNRAS* 366: 417–428
73. Falcke H, Körding E, Markoff S (2004) A scheme to unify low-power accreting black holes. Jet-dominated accretion flows and the radio/X-ray correlation. *A&A* 414: 895–903
74. Fanaroff BL, Riley JM (1974) The morphology of extragalactic radio sources of high and low luminosity. *MNRAS* 167: 31P–36P

75. Fedorenko VN, Courvoisier TJJ (1996) A model for radio/optical jets. *A&A* 307: 347–358
76. Feigelson ED, Laurent-Muehleisen SA, Kollgaard RI, Fomalont EB (1995) Discovery of inverse-Compton X-rays in radio lobes. *ApJ* 449: L149–L152
77. Feretti L, Fanti R, Parma P, Massaglia S, Trusconi E, Brinkmann W (1995) *ROSAT* observations of the B2 radio galaxies 1615+35 and 1621+38: implications for the radio source confinement. *A&A*, 298: 699–710
78. Forman WR, et al. (2007) Filaments, bubbles, and weak shocks in the gaseous atmosphere of M87. *ApJ* 665: 1057–1066
79. Gebhardt K, et al. (2000) A relationship between nuclear black hole mass and galaxy velocity dispersion. *ApJ* 539: L13–L16
80. Georganopoulos M, Kazanas D (2003) Relativistic and slowing down: the flow in the hot spots of powerful radio galaxies and quasars. *ApJ* 589: L5–L8
81. Georganopoulos M, Kazanas D (2004) Witnessing the gradual slowdown of powerful extragalactic jets: The X-ray-optical-radio connection. *ApJ* 604: L81–L84
82. Georganopoulos M, Kazanas D, Perlman E, Stecker FW (2005) Bulk comptonization of the cosmic microwave background by extragalactic jets as a probe of their matter content. *ApJ* 625: 656–666
83. Georganopoulos M, Perlman ES, Kazanas D, McEnery J (2006) Quasar X-ray jets: gamma-ray diagnostics of the synchrotron and inverse Compton hypothesis: the case of 3C 273. *ApJ* 653: L5–L8
84. Ghisellini G, Celotti A, Fissati G, Maraschi L, Comastri A (1998) A theoretical unifying scheme for gamma-ray bright blazars. *MNRAS* 301: 451–468
85. Ghisellini G, Celotti A (2001) The dividing line between FR I and FR II radio galaxies. *A&A* 379: L1–L4
86. Ginzburg VL, Syrovatski SI (1964) *The origin of cosmic rays*. Pergamon Press, Oxford
87. Giovannini G, Feretti L, Gregorini L, Parma P (1988) Radio nuclei in elliptical galaxies. *A&A* 199: 73–84
88. Giovannini G (2004) Observational properties of jets in active galactic nuclei. *Ap&SS* 293: 1–13
89. Giovannini G, Cotton WD, Feretti L, Lara L, Venturi T (2001) VLBI observations of a complete sample of radio galaxies: 10 years later. *ApJ* 552: 508–526
90. Gliozzi M, Sambruna RM, Brandt WN (2003) On the origin of the X-rays and the nature of accretion in NGC 4261. *A&A* 408: 949–959
91. Godfrey LEH, et al. (2008) A multi-wavelength study of the extremely high surface brightness hotspot in PKS 1421-490. *ApJ*: submitted
92. Gopal-Krishna, Wiita PJ (2000) Extragalactic radio sources with hybrid morphology: implications for the Fanaroff-Riley dichotomy. *A&A* 363: 507–516
93. Hardcastle MJ, Worrall DM (1999) *ROSAT* X-ray observations of 3CRR radio sources. *MNRAS* 309: 969–990
94. Hardcastle MJ, Worrall DM (2000) Radio, optical and X-ray nuclei in 3CRR radio galaxies. *MNRAS* 314: 359–363
95. Hardcastle MJ, Birkinshaw M, Worrall, DM (2001) A *Chandra* detection of the radio hotspot of 3C 123. *MNRAS* 323: L17–L22
96. Hardcastle MJ, Birkinshaw M, Worrall DM (2001) *Chandra* observations of the X-ray jet in 3C 66B. *MNRAS* 326: 1499–1507
97. Hardcastle MJ, Worrall DM, Kraft RP, Forman WR, Jones C, Murray SS (2003) Radio and X-Ray Observations of the Jet in Centaurus A. *ApJ* 593: 169–183
98. Hardcastle MJ, Harris DE, Worrall DM, Birkinshaw M (2004) The origins of X-Ray emission from the hot spots of FR II radio sources. *ApJ* 612: 729–748
99. Hardcastle MJ, Evans DA, Croston JH (2006) The X-ray nuclei of intermediate-redshift radio sources. *MNRAS* 370: 1893–1904
100. Hardcastle MJ, et al. (2008) New results on particle acceleration in the Centaurus A jet and counterjet from a deep *Chandra* observation. *ApJ* 670: L81–L84
101. Harris DE, Carilli CL, Perley RA (1994) X-Ray emission from the radio hotspots of Cygnus-A. *Nature* 367: 713–716
102. Harris DE, Krawczynski H (2002) X-ray emission processes in radio jets. *ApJ* 565: 244–255

103. Harris DE, Krawczynski H (2006) X-ray emission from extragalactic jets. ARAA vol 44, pp. 463–506
104. Harris DE, Krawczynski H, Taylor GB (2002) X-Ray detection of the inner jet in the radio galaxy 3C 129. ApJ 578: 60–63
105. Harris DE, Cheung CC, Biretta JA, Sparks WB, Junor W, Perlman ES, Wilson AS (2006) The outburst of HST-1 in the M87 jet. ApJ 640: 211–218
106. Heavens AF, Meisenheimer K (1987) Particle acceleration in extragalactic sources: the role of synchrotron losses in determining the spectrum. MNRAS 225: 335–353
107. Heywood I, Blundell KM, Rawlings S (2007) The prevalence of Fanaroff-Riley type I radio quasars. MNRAS 381: 1093–1102
108. Hoshino M, Arons J, Gallant YA, Langdon AB (1992) Relativistic magnetosonic shock waves in synchrotron sources — shock structure and nonthermal acceleration of positrons. ApJ 390: 454–479
109. Hwang U, Decourchelle A, Holt SS, Petre R (2002) Thermal and nonthermal X-Ray emission from the forward shock in Tycho’s supernova remnant. ApJ 581: 1101–1115
110. Isobe N, Tashiro M, Makishima K, Iyomoto N, Suzuki M, Murakami MM, Mori M, Abe K (2002) A *Chandra* detection of diffuse hard X-ray emission associated with the lobes of the radio galaxy 3C 452. ApJ 580: L111–L115
111. Janiuk A, Czerny B, Siemiginowska A, Szczerba R (2004) On the turbulent α -disks and the intermittent activity in active galactic nuclei. ApJ 602: 595–602
112. Jester S, Harris DE, Marshall HL, Meisenheimer K (2006) New *Chandra* observations of the jet in 3C 273. I. Softer X-ray than radio spectra and the X-ray emission mechanism. ApJ 648: 900–909
113. Jester S, Meisenheimer K, Martel AR, Perlman ES, Sparks WB (2007) Hubble Space Telescope far-ultraviolet imaging of the jet in 3C273: a common emission component from optical to X-rays. MNRAS 380: 828–834
114. Jordán A, et al. (2008) Low-mass X-ray binaries and globular clusters in Centaurus A. ApJ 671: L117–L120
115. Jorstad SG, Marscher Ap (2004) The highly relativistic kiloparsec-scale jet of the gamma-ray quasar 0827+243. ApJ 614: 615–625
116. Jorstad SG, Marscher Ap (2006) The X-ray and radio jets of quasars on kiloparsec scales. Astron. Nachr. 327: 227–230
117. Junkes N, Haynes RF, Harnett JI, Jauncey DL (1993) Radio polarization surveys of Centaurus A (NGC 5128). I — The complete radio source at 6.3 cm. A&A, 269: 29–38
118. Kaiser CR (2000) The environments and ages of extragalactic radio sources inferred from multi-frequency radio maps. A&A 362: 447–464
119. Kataoka J, Stawarz L (2005) X-ray emission properties of large-scale jets, hot spots, and lobes in active galactic nuclei. ApJ 622: 797–810
120. Kataoka J, et al. (2008) *Chandra* reveals twin X-ray jets in the powerful FR II radio galaxy 3C 353. ApJ 685: 839–857
121. Killeen NEB, Bicknell GV, Ekers RD (1988) The thermally confined radio source in NGC 1399. ApJ 325: 180–188
122. Komissarov SS (1994) Mass-loaded relativistic jets. MNRAS 269: 394–402
123. Körding EG, Jester S, Fender R (2006) Accretion states and radio loudness in active galactic nuclei: analogies with X-ray binaries. MNRAS 372: 1366–1378
124. Kraft RP, Vázquez SE, Forman WR, Jones C, Murray SS, Hardcastle MJ, Worrall DM, Churazov E (2003) X-Ray emission from the hot interstellar medium and southwest radio lobe of the nearby radio galaxy Centaurus A. ApJ 592: 129–146
125. Kraft RP, Hardcastle MJ, Worrall DM, Murray SS (2005) A *Chandra* study of the multi-component X-Ray emission from the X-shaped radio galaxy 3C 403. ApJ 622: 149–159
126. Kraft RP, Birkinshaw M, Hardcastle MJ, Evans DA, Croston JH, Worrall DM, Murray SS (2007) A radio through X-ray study of the hot spots, active nucleus, and environment of the nearby FR II radio galaxy 3C 33. ApJ 659: 1008–1021
127. Kraft RP, et al. (2008) Evidence for nonhydrostatic gas motions in the hot interstellar medium of Centaurus A. ApJ 677: L97–L100
128. Krawczynski H, et al. (2001) Simultaneous X-Ray and TeV gamma-ray observation of the TeV blazar Markarian 421 during 2000 February and May. ApJ 559: 187–195
129. Laing RA (1996) Brightness and polarization structure of decelerating relativistic jets. In: Hardee PE, Bridle AH, Zensus JA (eds) Energy transport in radio galaxies and quasars.

- ASP Conference Series 100 pp. 241–252
130. Laing RA, Bridle AH (2002) Dynamical models for jet deceleration in the radio galaxy 3C 31. *MNRAS* 336: 1161–1180
 131. Laing RA, Bridle AH (2002) Relativistic models and the jet velocity field in the radio galaxy 3C 31. *MNRAS* 336: 328–352
 132. Laing RA, Canvin JR, Bridle AH, Hardcastle MJ (2006) A relativistic model of the radio jets in 3C 296. *MNRAS* 372: 510–536
 133. Leahy JP, Muxlow TWB, Stephens PW (1989) 151-MHz and 1.5-GHz observations of bridges in powerful extragalactic radio sources. *MNRAS* 239: 401–440
 134. Leahy JP (1991) Interpretation of large scale extragalactic jets. In: Hughes PA (ed) *Beams and Jets in Astrophysics*. Cambridge University Press, pp. 100–186
 135. Leahy JP (2000) Atlas of radio sources. <http://www.jb.man.ac.uk/atlas/>
 136. Ledlow MJ, Owen FN (1996) 20 cm VLA survey of Abell clusters of galaxies. VI. Radio/optical luminosity functions. *AJ* 112: 9–22
 137. Longair MS (1994) *High Energy Astrophysics*. Cambridge University Press
 138. Lovelace RVE, Li H, Koldoba AV, Ustyugova GV, Romanova MM (2002) Poynting Jets from Accretion Disks. *ApJ* 572: 445–455
 139. Lovell JEJ, et al. (2000) VSOP and ATCA observations of PKS 0637-752. In: Hirabayashi H, et al. (eds) *Astrophysical Phenomena Revealed by Space VLBI*. ISAS, Japan, pp. 215–218
 140. Mack K-H, Klein U, O’Dea CP, Willis AG, Saripalli L (1998) Spectral indices, particle ages, and the ambient medium of giant radio galaxies. *A&A* 329: 431–442
 141. Marshall HL, Schwartz DA, Lovell JEJ et al. (2005) A *Chandra* survey of quasar jets: first results. *ApJS* 156: 13–33, and (2008), work in preparation
 142. Marshall HL, et al. (2001) Structure of the X-ray emission from the jet of 3C 273. *ApJ* 549: L167–L171
 143. Marshall HL, Miller BP, Davis DS, Perlman ES, Wise M, Canizares CR, Harris DE (2002) A high-resolution X-ray image of the jet in M87 *ApJ* 564: 683–687
 144. McNamara BR, Nulsen PEJ (2007) Heating hot atmospheres with active galactic nuclei. *ARA&A* 45: 117–175
 145. Meier DL (2001) The association of jet production with geometrically thick accretion flows and black hole rotation. *ApJ* 548: L9–L12
 146. Merloni A, Heinz S, Di Matteo T (2003) A fundamental plane of black hole activity. *MNRAS* 345: 1057–1076
 147. Miley G (1980) The structure of extended extragalactic radio sources. *ARAA* 18: 165–218
 148. Migliori G, Grandi P, Palumbo G, Brunetti G, Stanghellini C (2007) Radio lobes of Pictor A: an X-ray spatially resolved study. *ApJ* 668: 203–208
 149. Morganti R, Fanti R, Gioia IM, Harris DE, Parma P, de Ruiter H (1988) Low luminosity radio galaxies — Effects of gaseous environment. *A&A* 189: 11–26
 150. Muxlow TWB, Garrington ST (1991) Observations of large-scale extragalactic jets. In: Hughes PA (ed) *Beams and Jets in Astrophysics*. Cambridge University Press, pp. 52–99
 151. O’Dea CP (1998) The compact steep-spectrum and gigahertz peaked-spectrum radio sources. *PASP* 110: 493–532
 152. O’Dea CP, Mu B, Worrall DM, Kastner J, Baum S, de Vries WH (2006) *XMM-Newton* detection of X-ray emission from the Compact Steep Spectrum radio galaxy 3C 303.1. *ApJ* 653: 1115–1120
 153. Pacholczyk AG (1970) *Radio Astrophysics*. W.H. Freeman and Co., San Francisco
 154. Pearson TJ (1996) Observations of parsec-scale jets. In: Hardee PE, Bridle AH & Zensus TA (eds) *Energy transport in radio galaxies and quasars*. ASO Conference Series vol. 100, pp. 97–108
 155. Perlman ES, Biretta JA, Zhou F, Sparks WB, Macchetto FD (1999) Optical and radio polarimetry of the M87 jet at 0.2'' resolution. *AJ* 117: 2185–2198
 156. Perlman ES, et al. (2006) Optical polarimetry of the jets of nearby radio galaxies. I The data. *ApJ* 651: 735–748
 157. Pesce JE, Sambruna RM, Tavecchio F, Maraschi L, Cheung CC, Urry CM, Scarpa R (2001) Detection of an X-Ray Jet in 3C 371 with *Chandra*. *ApJ* 556: L79–LL82
 158. Quillen AC, Brookes MH, Keene J, Stern D, Lawrence CR, Werner MW (2006) *Spitzer* observations of the dusty warped disk of Centaurus A. *ApJ* 645: 1092–1101

159. Rafferty DA, McNamara BR, Nulsen PEJ, Wise MW (2006) The Feedback-regulated growth of black holes and bulges through gas accretion and starbursts in cluster central dominant galaxies. *ApJ* 652: 216–231
160. Rakowski CE, Ghavamian P, Hughes JP (2003) The physics of supernova remnant blast waves. II. Electron-ion equilibration in DEM L71 in the Large Magellanic Cloud. *ApJ* 590: 846–857
161. Rawlings S, Jarvis MJ (2004) Evidence that powerful radio jets have a profound influence on the evolution of galaxies. *MNRAS* 355: L9–L12
162. Readhead ACS, Taylor GB, Pearson TJ, Wilkinson PN (1996) Compact symmetric objects and the evolution of powerful extragalactic radio sources. *ApJ* 460: 634–643
163. Rees MJ (1971) New Interpretation of Extragalactic Radio Sources. *Nature* 229: 312–317 & erratum 510
164. Reynolds CS, Begelman MC (1997) Intermittent radio galaxies and source statistics. *ApJ* 487: L135–L138
165. Richstone D, et al. (1998) Supermassive black holes and the evolution of galaxies. *Nature* 395: A14–A19
166. Röser H-J, Meisenheimer K, Neumann M, Conway RG, Perley RA (2000) The jet of 3C 273 observed with *ROSAT* HRI. *A&A* 360: 99–106
167. Rossi P, Mignone A, Bodo G, Massaglia S, Ferrari I (2008) Formation of dynamical structures in relativistic jets: the FRI case. *A&A* 488: 795–806
168. Rybicki GR, Lightman AP (1979) *Radiative processes in astrophysics*. Wiley, New York
169. Sambruna RM, Urry CM, Tavecchio F, Maraschi L, Scarpa R, Chartas G, Muxlow T (2001) *Chandra* observations of the X-ray jet of 3C 273. *ApJ* 549: L161–L165
170. Sambruna RM, Maraschi L, Tavecchio F, Urry CM, Cheung CC, Chartas G, Scarpa RR, Gambill JK (2002) A survey of extended radio jets with *Chandra* and the Hubble Space Telescope: first results. *ApJ* 571: 206–217
171. Sambruna RM, Gambill JK, Maraschi L, Tavecchio F, Cerutti R, Cheung CC, Urry CM, Chartas G (2004) A survey of extended radio jets with *Chandra* and the Hubble Space Telescope. *ApJ* 608: 698–720
172. Sambruna RM, Gliozzi M, Donato D, Maraschi L, Tavecchio F, Cheung CC, Urry CM, Wardle JFC (2006) Deep *Chandra* and multicolor HST follow-up of the jets in two powerful radio quasars. *ApJ* 641: 717–731
173. Sambruna RM, Donato D, Cheung CC, Tavecchio F, Maraschi L (2008) A kpc-scale X-ray jet in the BL Lac source S5 2007+777. *ApJ* 684: 862–869
174. Sarazin CL (1986) X-ray emission from clusters of galaxies. *Rev. Mod. Phys.* 58: 1–115
175. Scheuer PAG, Readhead ACS (1979) Superluminally expanding radio sources and the radio-quiet QSOs. *Nature* 277: 182–185
176. Schoenmakers AP, de Bruyn AG, Röttgering HJA, van der Laan H, Kaiser CR (2000) Radio galaxies with a ‘double-double morphology’ - I. Analysis of the radio properties and evidence for interrupted activity in active galactic nuclei. *MNRAS* 315: 371–380
177. Schwartz DA, et al. (2000) *Chandra* discovery of a 100 kiloparsec X-ray jet in PKS 0637-752. *ApJ* 540: 69–72
178. Schwartz DA, et al. (2006) *Chandra* observations of magnetic fields and relativistic beaming in four quasar jets. *ApJ* 640: 592–602
179. Schwartz DA, et al. (2006) The X-ray jet and lobes of PKS 1354+195 (=4C 19.44). *Ap&SS* 311: 341–345
180. Schwartz DA, et al. (2006) Discovery of an X-ray jet and extended jet structure in the quasar PKS 1055+201. *ApJ* 647: L107–L110
181. Siemiginowska A, Bechtold J, Aldcroft TL, Elvis M, Harris DE, Dobrinska A (2002) *Chandra* discovery of a 300 kpc X-ray jet in the gigahertz-peaked spectrum quasar PKS 1127-145. *ApJ* 570: 543–556
182. Siemiginowska A, Smith RK, Aldcroft TL, Schwartz DA, Paerels F, Petric AO (2003) An X-ray jet discovered by *Chandra* in the $z=4.3$ radio-selected quasar GB 1508+5714. *ApJ* 598: L15–L18
183. Siemiginowska A, et al. (2003) *Chandra* discovery of an X-ray jet and extended X-ray structure in the $z = 0.63$ quasar B2 0738+313. *ApJ* 595: 643–655
184. Siemiginowska A, Cheung CC, LaMassa S, Burke DJ, Aldcroft TL, Bechtold J, Elvis M, Worrall DM (2005) X-Ray Cluster Associated with the $z = 1.063$ CSS Quasar 3C 186: The Jet is Not Frustrated. *ApJ* 632: 110–121

185. Sikora M, Sol H, Begelman MC, Madejski GM (1996) Radiation drag in relativistic active galactic nucleus jets. *A&AS* 120: 579–582
186. Sikora M, Madejski GM, (1996) Learning about Active Galactic Nucleus jets from spectral properties of blazars. *ApJ* 484: 108–117
187. Sivakoff GR, et al. (2008) A transient black hole low-mass X-ray binary candidate in Centaurus A. *ApJ* 677: L27–L30
188. Smith DA, Wilson AS, Arnaud KA, Terashima Y, Young AJ (2002) A *Chandra* X-ray study of Cygnus A. III. The cluster of galaxies. *ApJ* 565: 195–207
189. Spitzer L (1978) *Physical Processes in the Interstellar Medium*. Wiley, New York
190. Stanghellini C, O’Dea CP, Dallacasa D, Cassaro P, Baum SA, Fanti R, Fanti C (2005) Extended emission around GPS radio sources. *A&A* 443: 891–902
191. Stawarz L, Sikora M, Ostrowski M, Begelman MC (2004) On multiwavelength emission of large-scale quasar jets. *ApJ* 608: 95–107
192. Stawarz L, Cheung CC, Harris DE, Ostrowski M (2007) The electron energy distribution in the hotspots of Cygnus A: filling the gap with the Spitzer Space Telescope. *ApJ* 662: 213–223
193. Tagliaferri G, et al. (2003) The BL Lacertae objects OQ 530 and S5 0716+714. Simultaneous observations in the X-rays, radio, optical and TeV bands. *A&A* 400: 477–486
194. Takahashi Y, et al. (2000) Complex spectral variability from intensive multiwavelength monitoring of Markarian 421 in 1998. *ApJ* 542: L105–L109
195. Tashiro M, et al. (1998) Evidence of energy nonequipartition between particles and fields in lobes of the radio galaxy PKS 1343-601 (Centaurus B). *ApJ* 499:713–718
196. Tavecchio F, et al. (2000) Gamma-loud quasars: a view with BeppoSAX. *ApJ* 543: 535–544
197. Tavecchio F, Maraschi L, Sambruna RM, Urry CM (2000) The X-Ray Jet of PKS 0637-752: Inverse Compton Radiation from the Cosmic Microwave Background? *ApJ* 544: L23–L26
198. Tavecchio F, Ghisellini G, Celotti A (2003) Clumps in large scale relativistic jets. *A&A* 403: 83–91
199. Tavecchio F, Maraschi L, Sambruna RM, Gliozzi M, Cheung CC, Wardle JFC, Urry CM (2006) Deceleration from entrainment in the jet of the quasar 1136-135. *ApJ* 641: 732–739
200. Tavecchio F, Maraschi L, Wolter A, Cheung CC, Sambruna RM, Urry CM (2007) *Chandra* and HST observations of gamma-ray blazars: comparing jet emission at small and large scales. *ApJ* 662: 900–908
201. Tregillis IL, Jones TW, Ryu D (2001) Simulating electron transport and synchrotron emission in radio galaxies: Shock acceleration and synchrotron aging in three-dimensional flows. *ApJ* 557: 475–491
202. Tregillis IL, Jones TW, Ryu D (2004) Synthetic observations of simulated radio galaxies. I radio and X-ray analysis. *ApJ* 601: 778–797
203. Uchiyama Y, et al. (2007) An infrared study of the large-scale jet in quasar PKS 1136-135. *ApJ* 661: 719–727
204. Ueno S, Koyama K, Nishida M, Yamauchi S, Ward MJ (1994) X-ray observations of Cygnus A using the GINGA satellite. *ApJ* 431: L1–L4
205. Urry CM, Treves A, Maraschi L (1997) Multiwavelength monitoring of the BL Lacertae object PKS 2155-304 in 1994 May. III. Probing the inner jet through multiwavelength correlations. *ApJ* 486: 799–809
206. Varano, S, Chiaberge M, Macchetto FD, Capetti A (2004) The nuclear radio-optical properties of intermediate redshift FR II radio galaxies and quasars. *A&A* 428: 401–408
207. Verdoes Kleijn GA, Baum SA, de Zeeuw PT, O’Dea CP (2002) Core radio and optical emission in the nuclei of nearby FR I radio galaxies. *AJ* 123: 1334–1356
208. Wardle JFC, Aaron SE (1997) How fast are the large-scale jets in quasars? Constraints on both Doppler beaming and intrinsic asymmetries. *MNRAS* 286: 425–435
209. Weisskopf MC, Tananbaum HD, Van Speybroeck LP, O’Dell SL (2000) *Chandra* X-ray observatory (CXO): overview. In: Trümper, et al. (eds) *Proceedings of SPIE Vol 4012, X-Ray Optics, Instruments, and Missions III*, International Society for Optical Engineering, pp. 2–16
210. Williams AG (1991) Numerical simulations of radio source structure. In: P.A. Hughes (ed) *Beams and Jets in Astrophysics*. Cambridge University Press, pp. 342–378

211. Willott CJ, Rawlings S, Blundell KM, Lacy M (1999) The emission line-radio correlation for radio sources using the 7C Redshift Survey. *MNRAS* 309: 1017–1033
212. Wilson AS, Young AJ, Shopbell PL (2001) *Chandra* X-ray observations of Pictor A: High-energy cosmic rays in a radio galaxy? *ApJ* 547: 740–753
213. Wise MW, McNamara BR, Nulsen PEJ, Houck JC, David LP (2007) X-Ray supercavities in the Hydra A cluster and the outburst history of the central galaxy’s active nucleus. *ApJ* 659: 1153–1158
214. Worrall DM, Birkinshaw M (1994) Multiple X-ray emission components in low-power radio galaxies. *ApJ* 427: 134–139
215. Worrall DM, Birkinshaw M, Cameron RA (1995) The X-Ray environment of the dumbbell radio galaxy NGC 326. *ApJ* 449: 93–104
216. Worrall DM, Birkinshaw M (2000) X-Ray-emitting atmospheres of B2 radio galaxies. *ApJ* 530: 719–732
217. Worrall DM, Birkinshaw M, Hardcastle MJ (2001) *Chandra* finds that X-ray jets are common in low-power radio galaxies. *MNRAS* 326: L7–L12
218. Worrall DM, Birkinshaw M, Hardcastle MJ, Lawrence CR (2001) *Chandra* measurements of the X-ray core and cluster of 3C 220.1. *MNRAS* 326: 1127–1133
219. Worrall DM, Birkinshaw M (2005) X-ray synchrotron emission from the oblique shock in the jet of the powerful radio galaxy 3C346. *MNRAS* 360: 926–934
220. Worrall DM, Birkinshaw M (2006) Multiwavelength evidence of the physical processes in radio jets. *Lecture Notes in Physics* 693: 39–76
221. Worrall DM, Birkinshaw M, Laing RA, Cotton WD, Bridle AH (2007) The inner jet of the radio galaxy NGC 315 as observed with *Chandra* and the VLA. *MNRAS* 380: 2–14
222. Worrall DM, Birkinshaw M, Kraft RP, Hardcastle MJ (2007) The effect of a *Chandra*-measured merger-related gas component on the lobes of a dead radio galaxy. *ApJ* 658: L79–L82
223. Worrall DM, et al. (2008) Where Centaurus A gets its X-ray knottiness. *ApJ* 673: L135–L138
224. Young AJ, Wilson AS, Terashima Y, Arnaud KA, Smith DA (2002) A *Chandra* X-ray study of Cygnus A. II. The nucleus. *ApJ* 564: 176–189
225. Zezas A, Birkinshaw M, Worrall DM, Peters A, Fabbiano G (2005) *Chandra* observations of NGC 4261 (3C 270): revealing the jet and hidden active galactic nucleus in a Type 2 LINER. *ApJ* 627: 711–720